Master of Science in Mechanical Engineering

Untethered manipulation of electroactive polymer-actuator for soft robotics

소프트 로보틱스를 위한 전기 활성 폴리머 기반 액추에이터의 무선 조작

August 2023

Graduate School of Mechanical Engineering
Seoul National University
Design and Manufacturing Major

Kausthubharam

Untethered manipulation of electroactive polymer-actuator for soft robotics

Sung-Hoon Ahn

Submitting a master's thesis of
Mechanical Engineering

April 2023

Graduate School of Mechanical Engineering
Seoul National University
Design and Manufacturing Major

Kausthubharam

Confirming the master's thesis written by
Kausthubharam
June 2023

Chair	Heui Jae Pahk
Vice Chair	Sung-Hoon Ahn
Examiner	Howon Lee

Abstract

Ionic polymer metal composites are a type of Electroactive polymer that has received extensive attention over the past decade in soft robotics. This is attributed to favorable characteristics such as low input voltage and large displacement. However, critical drawbacks such as high hysteresis, back relaxation, and tethered power supply have limited their widespread usage in the micron domain. Thus the study aims to overcome these drawbacks by creating bending deformation of the ionic polymer membrane using a remote electric field. Parametrization study was performed to characterize the displacement and force developed by the proposed actuator. In addition, by incorporating a high charge-density ion into the polymer the performance is significantly improved. For instance, the tip force exerted by the ion-absorbed membrane increased by at least two times whereas the response speed increased by three times compared to the non-absorbed ionomer.

The proposed actuator was applied to two soft robotic applications. First, micro gripper with ionic polymer actuator that could demonstrate pick and place operation is developed. The micro gripper could grip and release objects varying from 1 to 3 mm in diameter. Besides micro robotic fish that could be manipulated to traverse complex path is demonstrated. The micro robot could achieve speeds up to 0.42 Bls^{-1} with tail and 0.96 Bls^{-1} without tail.

The proposed actuator is anticipated to have huge potential in the field of soft robotics. We further envision its usage in the biomedical field and lab-on-chip systems for therapeutic drug delivery and manipulation of biological specimens.

Keyword : Electroactive polymer, IPMC, untethered actuation, electric field, soft robotics
Student Number : 2021-29633

Acknowledgement

I would like to express the deepest gratitude to my advisor Prof. Sung-Hoon Ahn for providing me with the amazing opportunity to conduct research at IDIM Laboratory. I am very grateful for his constant guidance and encouragement throughout my Master's degree.

I am thankful to all my lab mates for providing tremendous support and assistance during research.

Lastly, I would like to thank my parents for their unconditional love and support.

Table of Contents

List of Figures

List of Tables

Nomenclature

Description	Symbol	Unit
Cation concentration	C	mol/m^3
Diffusion coefficient	D	m^2/s
Faraday's constant	F	C/mol
Cation mobility	μ	$m^2/(sV)$
Electric potential	φ	V
Charge density	ρ	VF/m^2
Dielectric permittivity	ε	F/m
Current density	J	A/m^2
Electrical conductivity	σ	S/m
Mass flux	Q	$Kg/(m^2s)$
Permeability	K	N/A^2
Pressure gradient	∇p	Pa/m
Coupling coefficient	A_{xy}	-
Young's modulus	Y_E	Pa

Bending torque	τ	Nm
Radius of curvature	R	m
Bending constant	P	m/kg
Electric field	E	V/m
Ionic mobility	μ	$m^2/(Vs)$
Charge number	Z	-
Elementary charge	e	C
Hydrodynamic radius	r	m
Viscosity	η	Pas
Drift velocity	v	m/s

Chapter 1. Introduction

1.1. Background

Development of robotic systems to automate processes is always a pioneering topic in engineering. However conventional robots consist of motors and links which make them rigid and not capable of manipulating fragile objects. To overcome this extensive research on the development of smart materials and systems that mimic natural muscles is conducted since the late 90s [1-3]. Currently, there exists a wide array of smart materials that respond mechanically to different environmental stimuli such as heat, electricity, light, and magnet [Figure 1.1]. From an array of such materials, polymers that deform on supplying an electric field are called Electroactive polymers (EAPs). When compared to other smart materials EAPs exhibit large strain, low weight, high flexibility thus making them an ideal candidate for the manipulation of delicate objects [Table 1.1][4]. Further, since the force developed by EAPs is similar to natural muscles they are usually called Artificial muscles [5]. Based on the actuation mechanism EAP actuators are broadly classified into Field-activated EAP and ionic EAP. Field activated EAP consists of dielectric polymer coated with electrodes and when voltage is applied between the electrodes results in the generation of Maxwell stress consequently deforming the entire structure. Field-activated EAPs have high response speed and high power density but they require very high input voltage making them highly inefficient. Whereas ionic EAPs usually have a polyelectrolyte membrane that is coated by electrodes and the deformation is a result of the diffusion of ions in the polymer [6]. Amongst different ionic EAPs, IPMC or ionic polymer metal composites is extensively studied. The structure of IPMC consists of an ion-exchange membrane which is coated on both sides by electrodes [7-9]. The advantage of IPMC over field-activated EAPs is that they undergo large displacement on the application of low voltage. Thus over the past decade, IPMC has been actively researched in soft robotics and consequently resulting in the development of grippers, actuators, mobile robots, and even sensors [10-15].

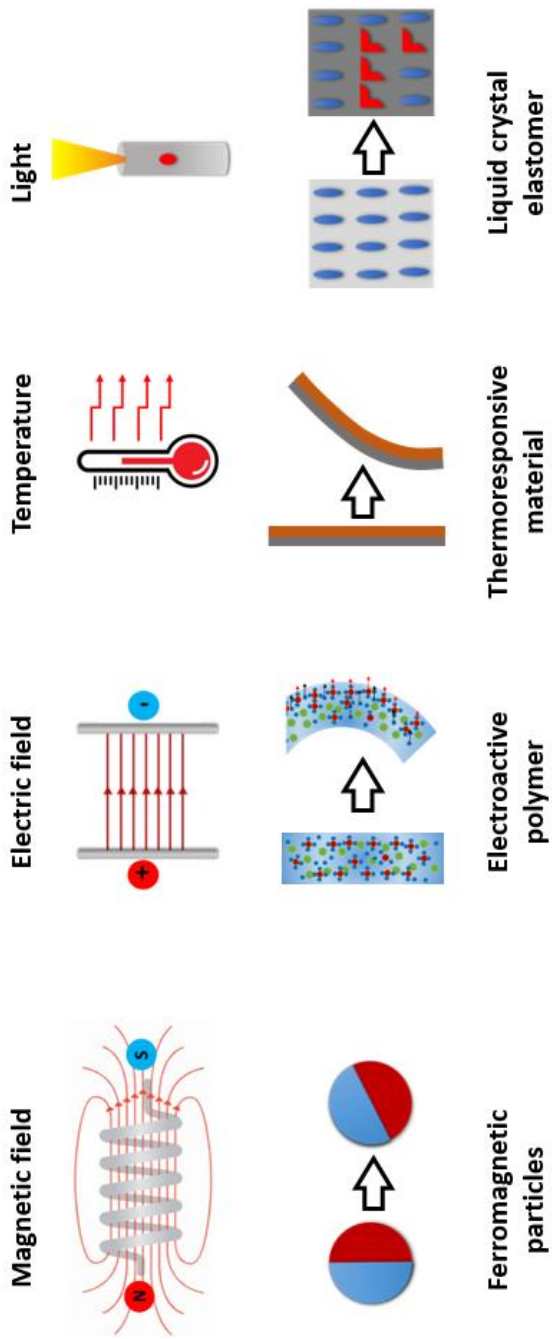

Figure 1.1. Schematics representing the various smart materials that respond to different input stimuli.

Table 1.1. Comparison of performance of different smart materials [4].

Smart Materials	Strain (%)	Stress (MPa)	Efficiency (%)
Piezoelectric	0.09	35	>30
SMA	>5	>200	>3
Magnetostrictive	0.2	70	<30
Electrostatic	>10	0.04	>20
IPMC	>40	0.3	>30

Despite the popularity of IPMC, currently they face a few critical drawbacks such as back relaxation, high hysteresis, and tethered power supply. These have hindered their implementation beyond the lab environment.

1.2. Motivation

Previously it was reported that despite supplying constant input voltage after the instantaneous displacement it relaxes towards the original position. This decrease in displacement is termed back relaxation. Over the years many theories are proposed to explain this observation. However, the widely accepted reason is that osmotic pressure that generates the bending movement of the IPMC will eventually move the water molecules back to their original position thus reducing the displacement. In addition to this IPMC also displays high hysteresis. That is the performance of IPMC is observed to decrease drastically in a short time due to evaporation of water from the cracks present on the electrode surface. Finally, IPMC required tethered connection to supply voltage which restricts its application scope.

The current state to solve back relaxation includes either implementing a

feedforward loop system with patterned electrodes [16]. Further back relaxation was mitigated without electrode patterning and a closed loop system by incorporating local Gaussian noise [17]. The current solution for water evaporation includes coating the surface of IPMC using passive layers such as PDMS and PET [18, 19]. Further few studies have also reported that the working time of IPMC can be improved by coating the surface with an extra layer of electrode [20]. Another solution includes exchanging water with ionic liquid which has a considerably low evaporation rate [21]. To solve this issue of tethered connection studies typically use onboard battery and control circuit to receive remote power. Further Chang et al. [22] implemented resonance coupling of electromagnetic signal to supply untethered power to IPMC through the use of an external magnetic field generator and onboard RF signal receiver.

1.3. Purpose of Research

In the last session, the drawbacks of IPMC and current state-of-the-art solutions were highlighted. However current methods create some unwanted problems. For instance, the solutions to mitigate the back relaxation such as closed loop system and noise signal increase the complexity of the system decreasing the feasibility of practical implementation. Further passive layer coating of IPMC increases its section modulus consequently reducing the performance. On the other hand, replacing water with ionic liquid reduces the response speed of IPMC [23]. Finally incorporating an RF signal receiver and battery increases system weight and causes scaling issues during the miniaturization, thus restricting the usage of IPMC in the microdomain.

Thus the objective of the study was to solve this issue without increasing complexity or weight thus improving the feasibility for usage in the biomedical field. We were able to create usable bending movement in the ionic polymer which was immersed in the electrolyte by using a remote low electric field. This is a significant contribution as unlike previous research this method provides untethered power supply without adding extra components to the system. It must be noted that there are few studies on the untethered actuation of electroactive hydrogel using an electric field [24]. However, the previously reported actuators required a high electric field (0.5 – 0.6 V/mm)

and had a very slow response (of several minutes), thus restricting its practical implementation. On the other hand, the actuator developed in this study has a response speed of less than 5 seconds and requires an electric field with a strength of 0.1 V/mm. Further, unlike IPMC, the developed actuator could hold its displacement for a long time under a constant low electric field. Due to its simplicity and wireless power delivery, the developed actuator is expected to have huge potential in the biomedical field.

Chapter 2. Principle of actuation

2.1. Mechanism of IPMC deformation

As depicted in figure 2.1 IPMC consists of an ionic membrane that is coated on both sides by electrodes. Due to the popularity of IPMC as an actuator and sensor numerous models have been proposed to explain the bending characteristic. Based on the theoretical foundation used to model the deformation of IPMC, models can be broadly classified into physics-based modeling and equivalent circuit model (EQM) [25, 26]. In physics-based model, partial differential equations and complete coupling of the electrochemomechanics that govern the deformation is studied. In such models, ionic polymer is considered as consisting of inverted micellar structure interconnected with nanosized channels through which the transport of mobile ions occurs. Thus the diffusion of ions is modeled using Nernst-Plank equation (equation 2.1) whereas the coupling between the diffusion of ions and mechanical deformation is modeled using Poisson's equation (equation 2.2). They can be written as,

$$\frac{\partial C}{\partial t} + \nabla.(-D\nabla C - z\mu FC\nabla\varphi) = 0 \tag{2.1}$$

$$\nabla.\ \vec{E} = -\nabla^2\varphi = \frac{\rho}{\varepsilon} \tag{2.2}$$

Over the years, more complicated and fully coupled theories trying to explain the underlying physics have been developed. However, the complexity and computational expensiveness makes physics-based modeling unfavorable for practical application. On the other end, the simplicity and ease of application of the EQM have resulted in their implementation for real-time control [26]. In EQM, IPMC is viewed as a component of an electrical circuit. Thus, the surface electrodes are considered serial resistors, and the ionic polymer as parallel resistors and capacitors are connected in series. That said it is widely accepted that the deformation of IPMC is mainly due to the movement of hydrated ions through polymer structure on the supply of electric field. To delineate, the ionic polymer in IPMC is made of polymers having ionic end groups. In this end group, if the ionic polymer is Nafion then

the negative ion is fixed to polymer backbone and the positive is free to move under electric field. Thus on supplying an electric field between the surface coated electrodes the mobile cations move towards the negative electrode. However, since the cations in the ionomer are hydrated they drag water molecules with them. Due to the movement of water molecules swelling takes place near the negative electrode whereas contraction occurs at the positive, consequently causing the IPMC to bend towards the positive electrode (Figure 2.1).

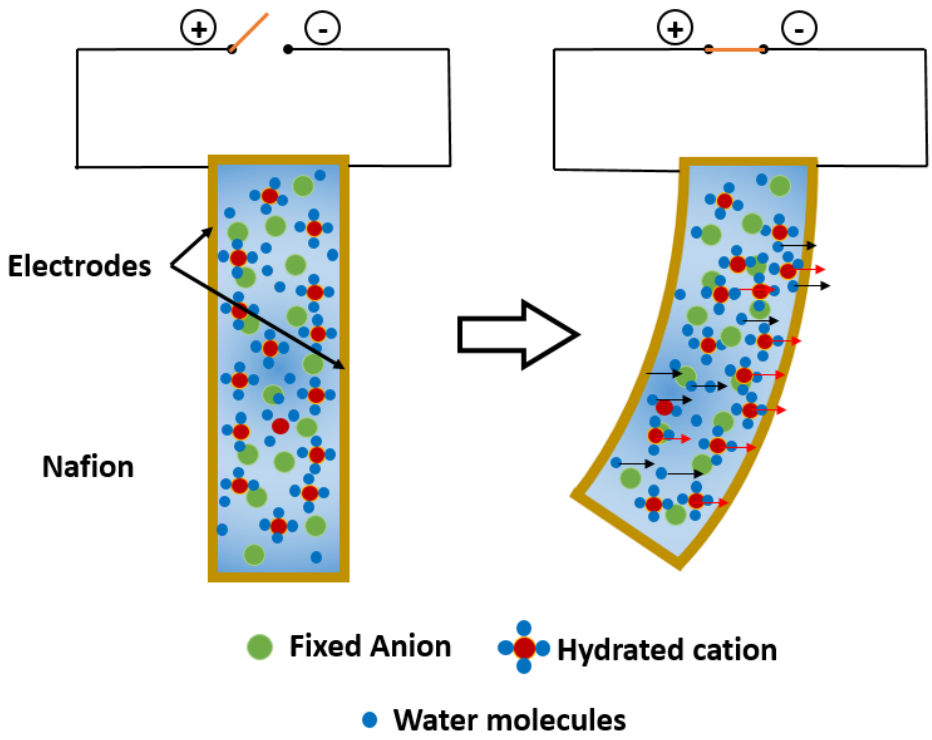

Figure 2.1. Schematics representing the deformation of IPMC on the application of voltage.

2.2. Actuation mechanism of ionomer

Whereas, it is observed that the ionomer deforms towards the negative electrode on supplying an electric field through the electrolyte solution (Figure 2.2(a)). This interesting behavior can be explained by two physical processes: Electrophoresis and osmosis. Electrophoresis is the phenomenon

of ion diffusion observed in a dispersed fluid medium under an external electric field. Thus it is the governing force for the transport of mobile ions inside the ionomer membrane. Further osmosis as known is the flow of solvent particles from a region of higher potential to lower when separated by a semi-permeable membrane. Osmotic pressure potential is the driving force for the movement of water molecules between the solution and the ionomer. Generally, these two physics are coupled by the Onsager relationship which is given as [27],

$$J = \sigma E - A_{12}\nabla p \tag{2.3}$$

$$Q = A_{12}E - K\nabla p\mathrm{t} \tag{2.4}$$

The nomenclature of terms is provided in the nomenclature section. Since pressure gradient is the dominant physics that causes the bending of the ionomer, bending curvature can be written as,

$$\frac{1}{R} = \frac{\nabla p}{kY_E} + \frac{12\tau(1-\vartheta^2)}{Y_E t^3} \tag{2.5}$$

Finally combining the above equation with governing equations (2.3 and 2.4) for ion and solvent transport gives the torque experienced by the ionomer during deformation as,

$$\tau = \frac{\nabla pP}{kY_E} = \frac{1}{12}\frac{(1-2\vartheta)}{(1-\vartheta)}\frac{Lh^3}{K}E \tag{2.6}$$

The reason behind the opposite deformation of the ionomer can be explained as follows. Before supplying an electric field, the ionomer is in Donnan equilibrium with the surrounding electrolyte solution [28]. This means that the osmotic pressure on both sides of the ionomer is similar due to the equal of contribution of water molecules. On the application of field, the mobile cations in the ionomer along with water molecules move towards the negative electrode which is similar to the IPMC. However, due to this motion, the concentration of water molecules inside the ionomer near the positive electrode region decreases consequently creating a high osmotic pressure in this region. This osmotic pressure causes the water from the solution to

diffuse into the ionomer and create swelling of this region (negative electrode). In contrast, near the negative electrode region the high concentration of water molecules inside the ionic polymer, pushes them out of the membrane into the solution subsequently resulting in the contraction of this region. Due to the combined effect of swelling and contraction, it is observed that the ionomer bends toward the negative electrode region as shown in figure 2.2(b).

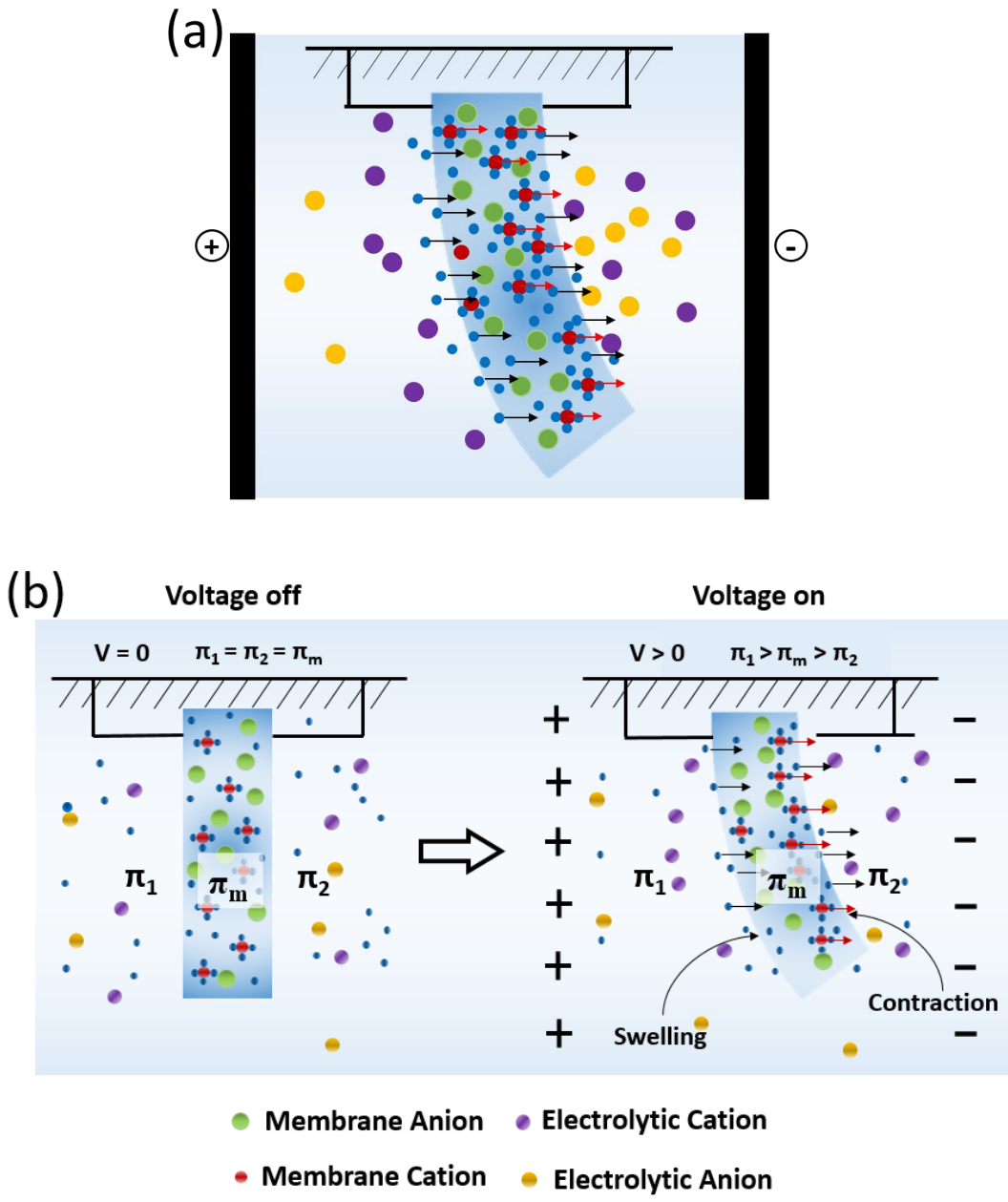

Figure 2.2. Schematics of the (a) ionomer deforming towards to the negative electrode on the supply of electric field and (b) underlying physics that causes the observed deformation of IPMC.

Chapter 3. Experimental methods

3.1. Fabrication of ionomer

The ionomer membrane was fabricated by the solution casting as shown in figure 3.1. The process involves casting a predetermined quantity (depending on the desired final thickness) of 5% wt Nafion solution into a glass petridish. Then the casted solution was heated at 70ºC for 6 hrs. at constant pressure and humidity. After the curing to improve the mechanical strength, the casted membrane was annealed at a temperature of 120ºC for 3 hrs. Finally, the annealed membrane was peeled from the pertidish by immersing the entire structure in DI water. During the annealing process, it was noted that the thickness of the membrane further decreases due to the evaporation of additional water molecules. To offset this difference, extra volume was added at the beginning of the casting solution which in turn improved the expected thickness of the final ionomer membrane (Figure 3.2).

3.2. Laser machining

The final actuator was obtained by laser machining of the ionomer membrane. For this purpose, a nanosecond UV pulse laser was used. Since the ionomer (nafion) is a polymer, it is inherently a bad conductor of heat resulting in a large heat affected zone during laser machining. Therefore, an optimization study of the laser parameters was done in order to obtain the least possible heat affected region (Figure 3.3). First, the unablated width of the ionomer actuator was tested with laser scan speed. It is observed that as expected the width of the ionomer increased with an increase in scan speed. This is because the laser power density decreases with increase of laser speed consequently reducing the heat affected zone. However, it is observed that the relationship is nonlinear. That is at higher scan speed the increment in the unablated region reduces. In addition to this, the effect of incrementing the laser scans on the width of the ionomer was investigated. It is observed that increasing the number of cycles decreases the unablated width with the rate of decrease being maximum at the lower number of cycles.

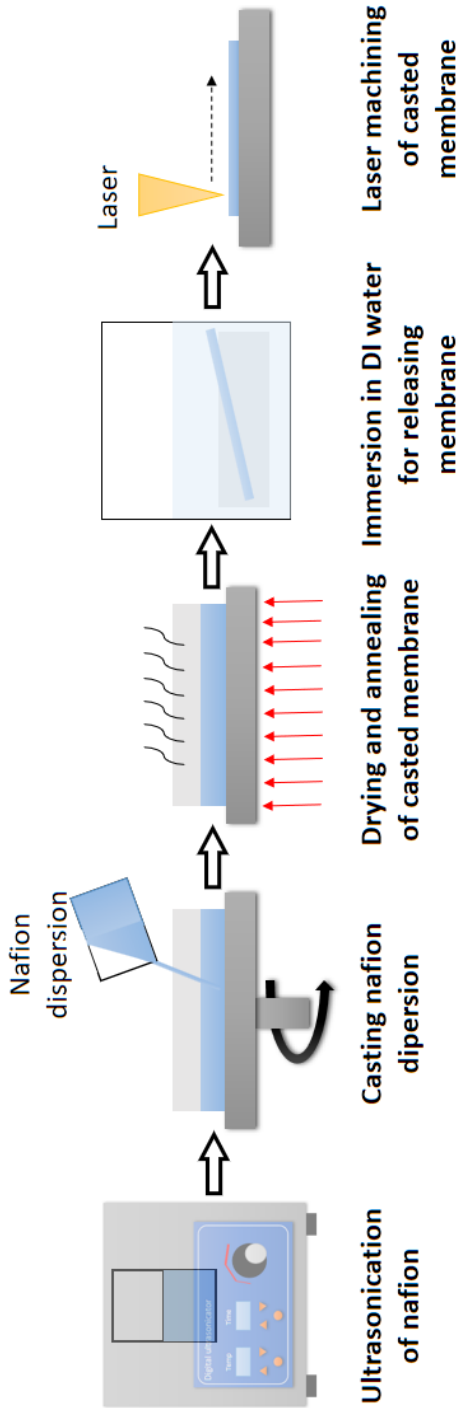

Figure 3.1. Schematics of solution casting process of the ionomer membrane

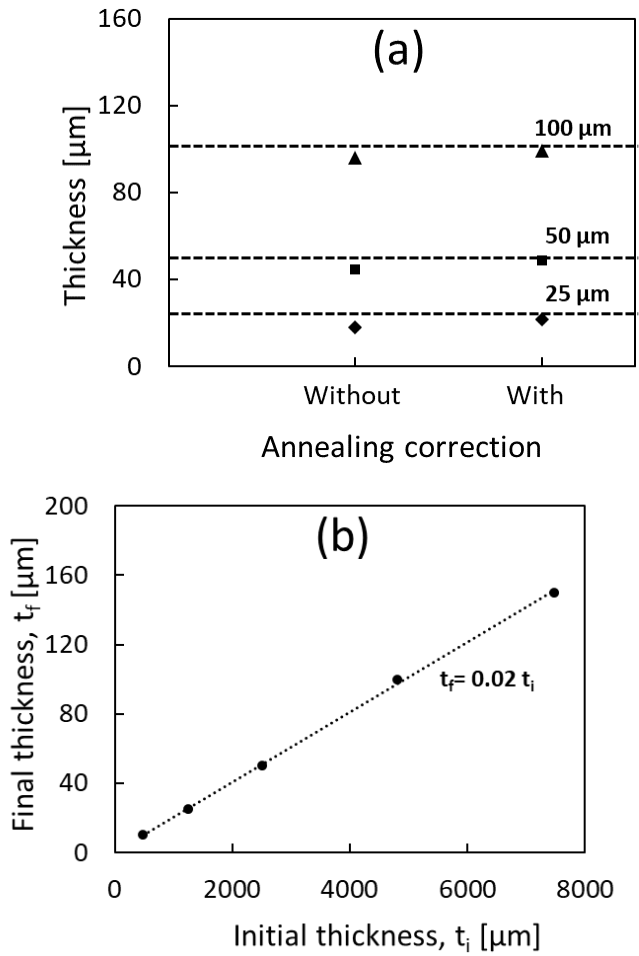

Figure 3.2. Thickness of the final ionomer membrane with (a) comparing final thickness with and without annealing correction and (b) relating the initial thickness required for attaining the desired final thickness

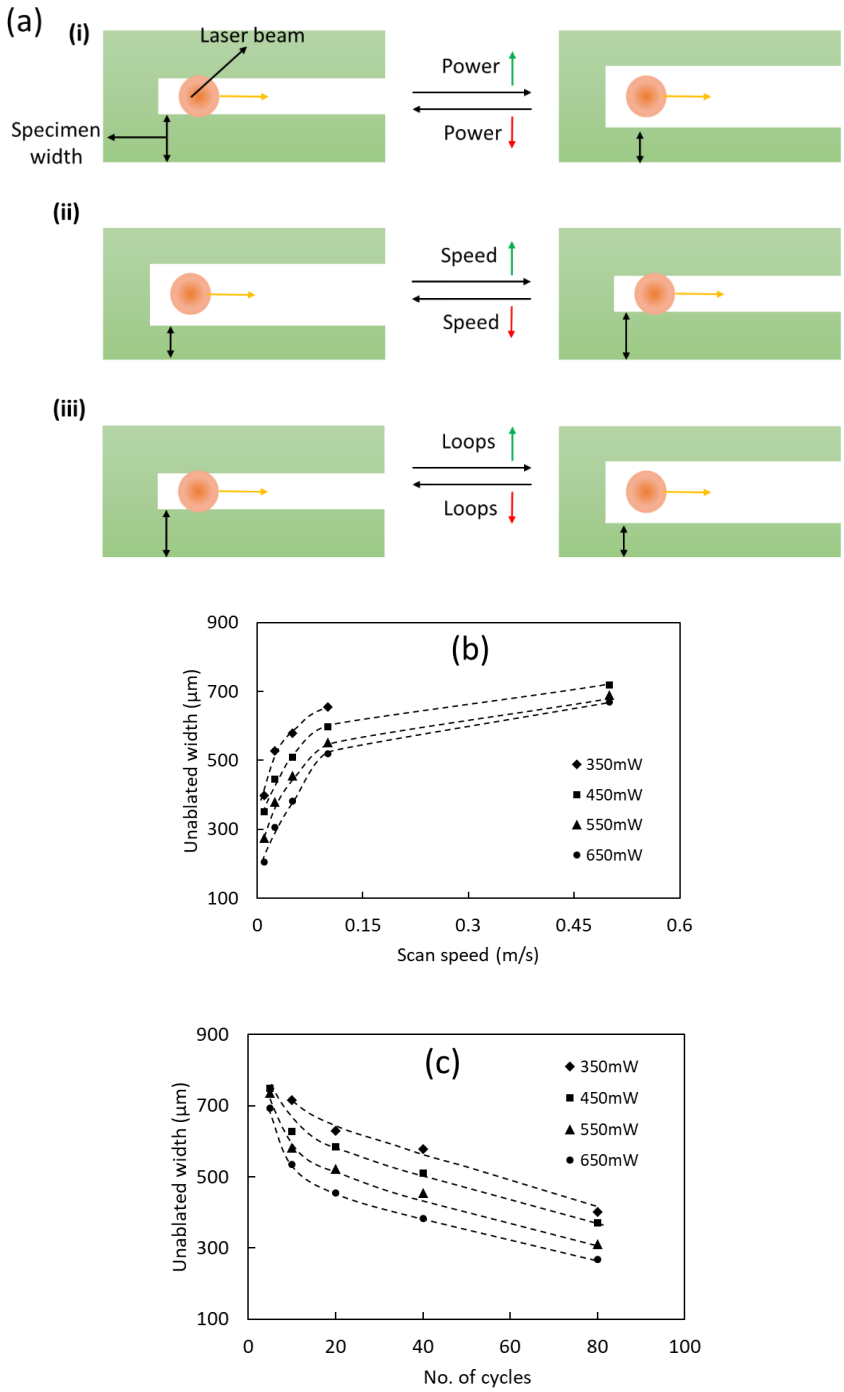

Figure 3.3. Laser machining. (a) Schematics of the effect of different laser parameters on the width of the specimen; (b) Relationship between unablated width and the laser scan speed; (c) Relationship between width of the actuator and the number of cycles for various laser powers.

3.3. Reversible ion-absorption process

In addition to fabricating the polymer, an ion-absorption process was implemented to incorporate high-charge density ions into the ionomer. For this purpose, an in-house experimental setup was fabricated based on the concept of the electrochemical cell. As shown in figure 3.4, the setup consisted of an ionic polymer membrane sandwiched between two electrodes having different galvanic potentials. In this study positive electrode was made of copper whereas the negative electrode was made of aluminum. These electrode materials were considered based on their availability and since we wanted to incorporate Cu-ions into the ionomer. To obtain an optimal parameter, the time of absorption and pH of the solution was varied and the results are provided in figure 3.5 (The hue values are calculated by using Matlab®). On supplying a low oxidative voltage of 5V to the positive electrode, it is observed that cupric ions were completely absorbed into the ionomer within 30 minutes. It must be noted that the entire setup was immersed in a water bath to keep the ionomer hydrated and avoid unnecessary bending. Further, the absorption of Cu-ions can be completely reversed by immersing the ionomer into the 0.1 M HCl solution for 12 hrs at room temperature.

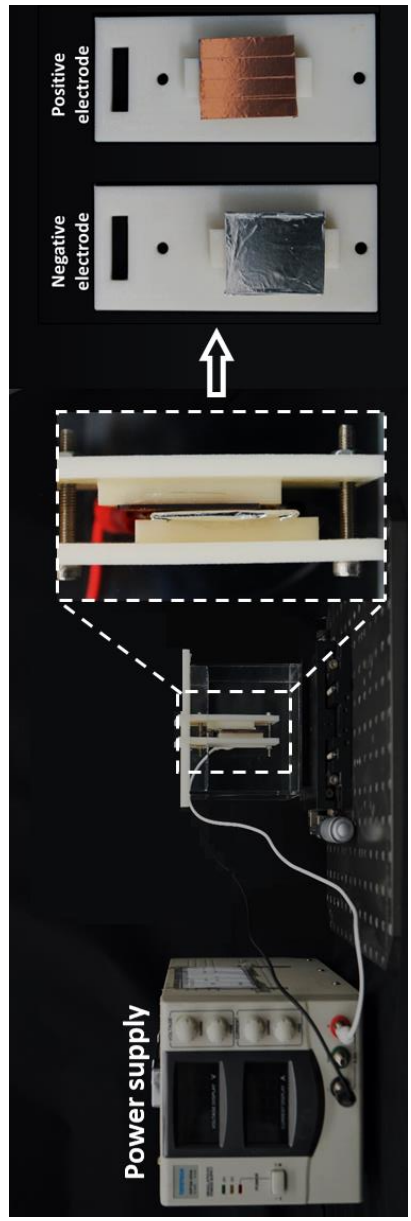

Figure 3.4. Experimental setup for the ion-absorption process

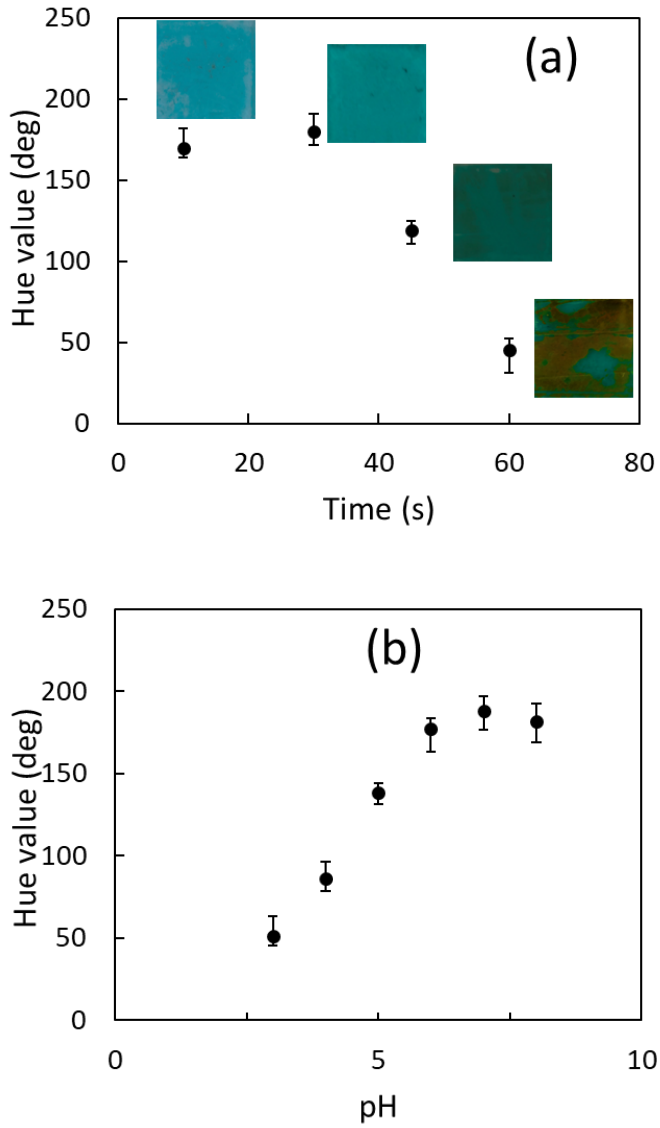

Figure 3.5. Quantification of the Cu-absorption by the ionomer by calculating the hue value at (a) Different time and (b) pH of the solution

Chapter 4. Results and Discussions

4.1. Response of ionomer to DC signal

The developed actuator was characterized for displacement under a DC signal. The experimental setup for the displacement characterization of the ionomer is shown in Figure 4.1. The setup consisted of the ionomer immersed vertically in an electrolyte bath made of sodium chloride (NaCl). Further graphite electrodes were used to supply remote electric field and the deformation of the ionomer was recorded using a CMOS camera. Further, it must be noted before conducting the experiment the ionomer was immersed in a NaCl bath to achieve equilibrium.

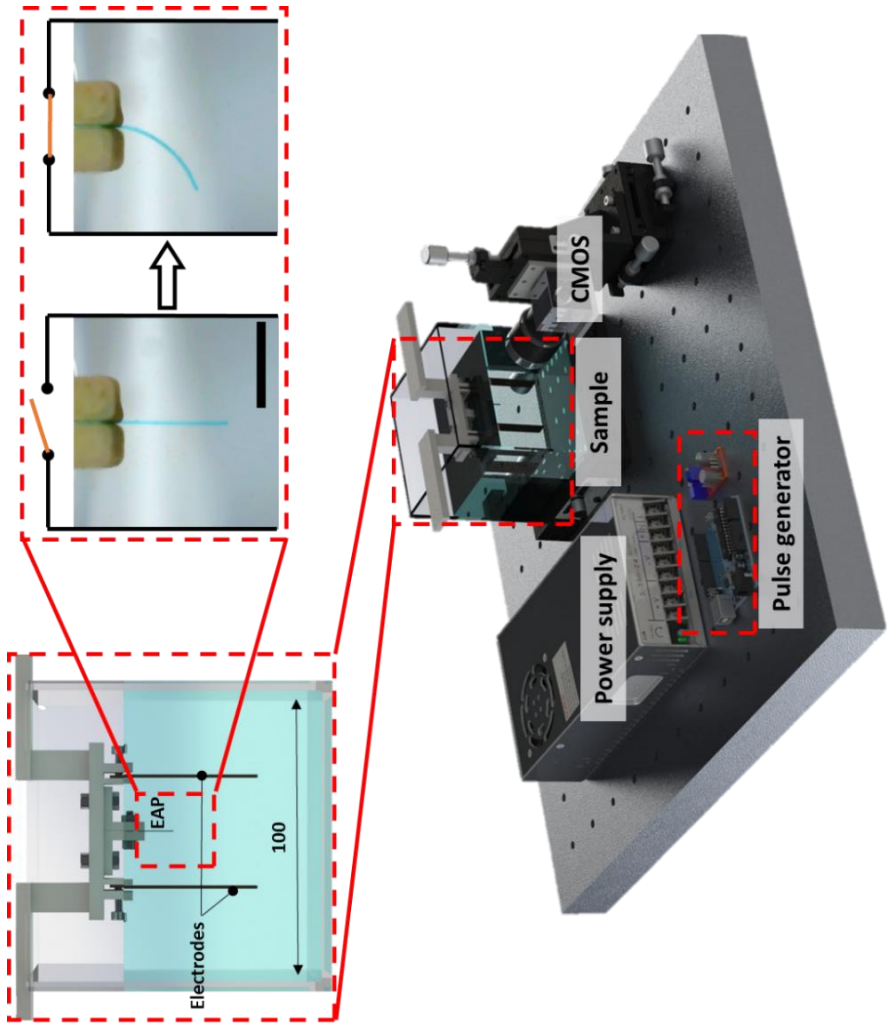

Figure 4.1. Schematics of the experimental setup for the displacement characterization of the ionomer actuator (both AC and DC). The insert is the experimental image of ionomer tip displacement. (Here scale bar is 5mm)

4.1.1 Effect of actuator width

It must be noted that the ionomer actuator was characterized before and after the ion-absorption process to investigate the improvement in performance after the incorporation of high-charge density ions (section 4.1.4.). First, the effect of width on the bending behavior of the ionomer was investigated. It is observed that the width of the actuator has minimal effect on the ionomer

deformation (Figure 4.2(a)). However, the response speed is observed to increase with the decrease in actuator width (Figure 4.2(b)). This can be attributed to the orientation of the ionomer where the width of the actuator is parallel to the electrode face. However, decreasing actuator width reduces its section modulus hence the improvement observed in the actuation speed.

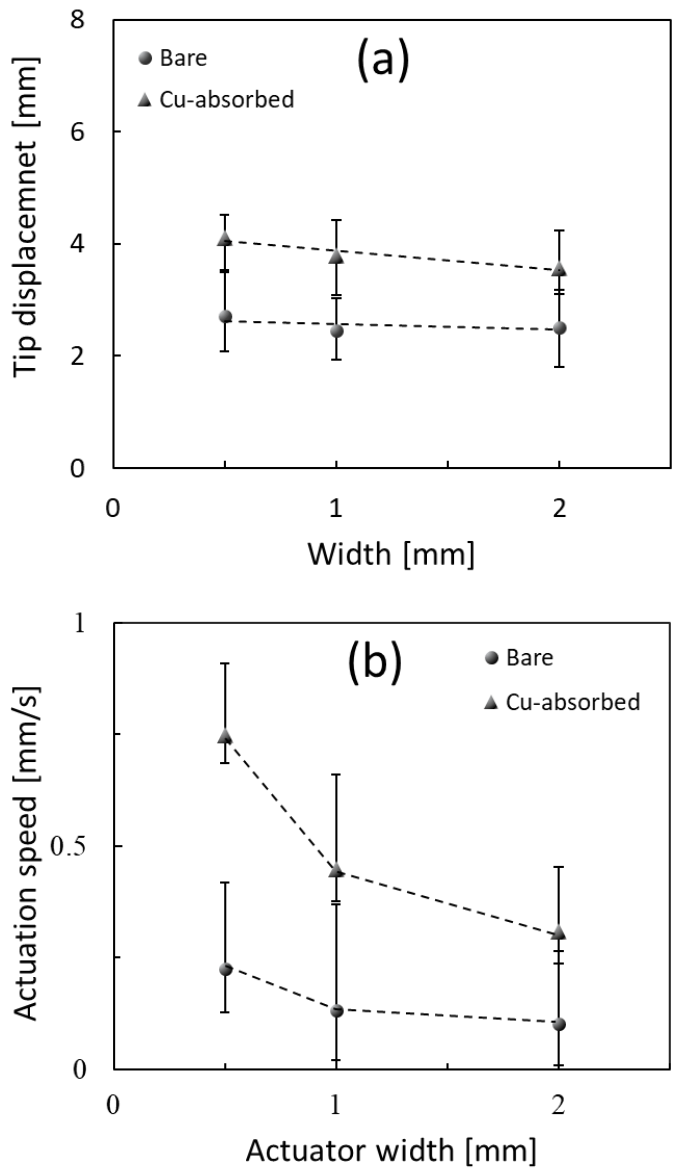

Figure 4.2. Effect of width of the ionomer on the (a) tip displacement and (b) actuation speed

4.1.2 Effect of actuator thickness

Further, the effect of the thickness of the actuator is investigated. Contrary to general expectation, it is observed that the bending magnitude of the ionic polymer increases with a decrease in the thickness value until a certain value (figure 4.3(a)). Beyond this thickness value, the tip displacement of the actuator is noted to decrease despite the decrease in the thickness. This interesting behavior can be attributed to the decrease in the number of mobile ions inside the ionomer with thickness. It is expected that amount of cations in the ionomer plays a significant role since the driving mechanism of the ionomer is based on the osmotic pressure generated by the movement of hydrated cations. Therefore, despite the thin ionomer having a low section modulus, decreasing the thickness value beyond a certain value lowers the quantity of these hydrated ions that it causing negative effect on the tip displacement produced. These opposing effects are schematically represented in Figure 4.3(b).

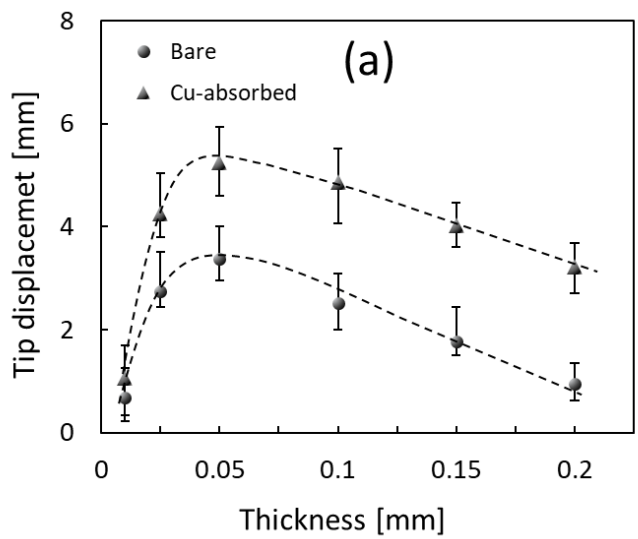

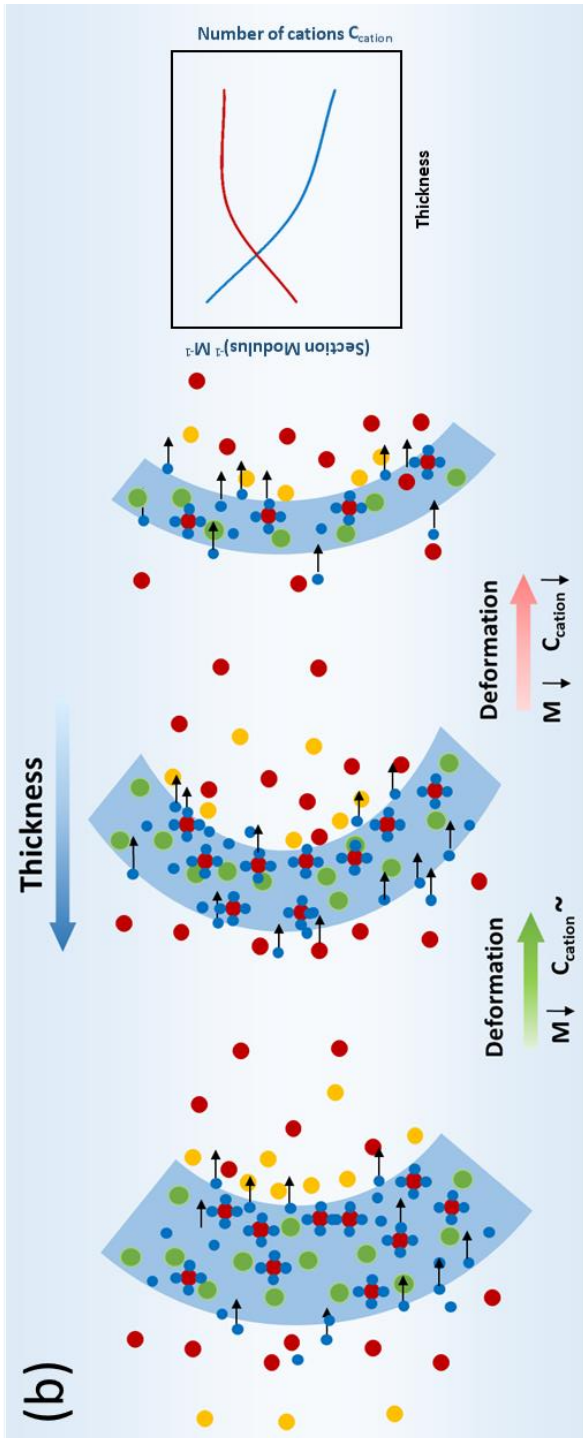

Figure 4.3. Effect of the thickness of the actuator on (a) the tip displacement and (b) schematics representing the relation of section modulus and number of cations with actuator thickness.

4.1.3 Effect of operational parameters

Besides structural optimization, the effect of operational parameters such as remote electric field and electrolyte salt concentration on the deformation behavior of the ionomer was studied. First, the effect of electric field is considered. It can be observed that as expected, the electric field has a linear relationship with the tip displacement produced by the actuator. Increasing the electric field applied through the remote electrodes increases the electrostatic forces acting on the mobile cations thus increasing their diffusion speed through the ionomer actuator (Figure 4.4).

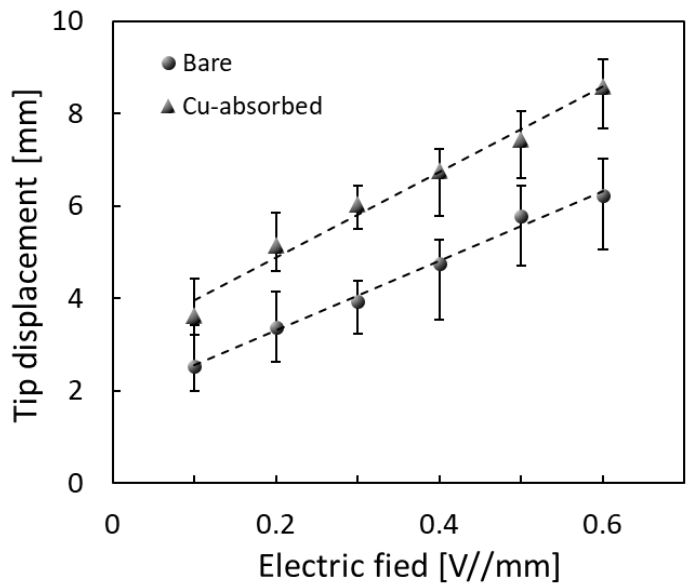

Figure 4.4. Tip displacement of the ionomer actuator with the electric field strength displays a linear relationship.

Further, as the concentration of the electrolyte bath is expected to affect the tip displacement achieved by the ionic polymer, various salt concentrations ranging from 0 to 1 M are considered. It is noted that the deformation of the actuator increases with increase in a salt concentration of 0.25 M beyond which the deformation reached decreases. This result in turn depicts that diffusion of water molecules between the ionomer and the solution has a major contribution towards the deformation of the ionomer. To delineate, it is

anticipated that the electrical conductivity of the salt increases with concentration as the charge density of ions in the solution increases. On the other hand, increasing salt concentration decreases the number of water molecules present per unit volume. This in turn reduces the quantity of water molecules that can move between the ionomer and electrolyte consequently decreasing the tip displacement of the actuator (Figure 4.5).

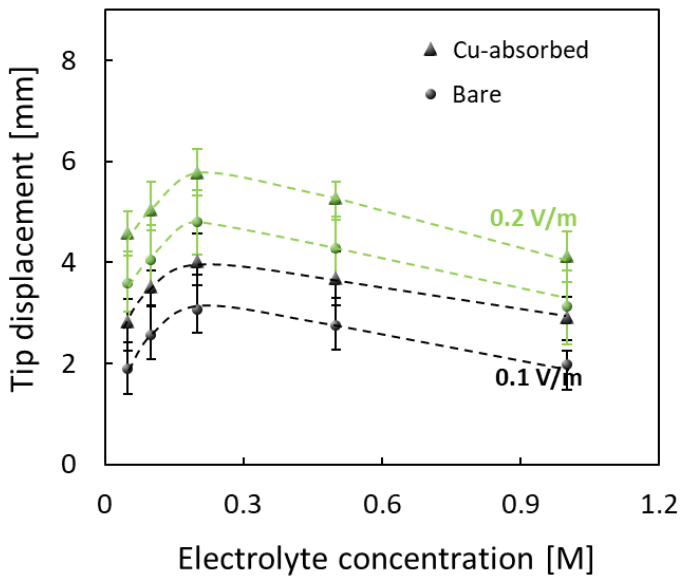

Figure 4.5. Effect of electrolyte concentration on deformation of ionomer wherein the tip displacement of ionomer decreases with an increase in salt concentration despite the increase in the electrical conductivity.

4.1.4 Effect of ion-absorption process

In this section, the effect of incorporating high charge density (Cu^{2+} ion) into the ionomer is studied. As seen from the figures, though the trend of results remained similar, including the ion absorption process significantly improved the performance of the actuator. For instance, as observed in Figure 4.2, the response speed of the Cu-absorbed ionomer is almost three times that of the bare actuator. Further, the tip displacement of the actuator after the incorporation of Cu-ions increased by at least 40% irrespective of the applied voltage, salt concentration, and dimension of the actuator. The reason for this

observed increase in the performance of the ionomer after the ion-absorption is delineated below.

First, cupric ion has higher charge density compared to sodium ion. Due to this under an electric field copper ions experience almost two times electrostatic force. Further, the hydrodynamic radius of copper ions is less than sodium ions [29]. The combined effect of higher electrostatic force and lower hydrodynamic radius enables the copper ions to move through the ionomer membrane at a faster rate, thus increasing the response speed of the Cu-absorbed ionomer compared to the non-absorbed counterpart. Theoretically, ions in dispersed medium experience electrostatic force and a retardation force which are given as,

$$F_{field} = ZeE \tag{4.1}$$

$$F_{retardation} = 6\pi\eta r v \tag{4.2}$$

Equating the above equations gives the mobility of ions as,

$$\mu = \frac{eZ}{6\pi\eta r} \tag{4.3}$$

Thus from equation 4.3, it is observed that ions with higher charge density and lower hydrodynamic radius will have higher mobility thus validating our reason for the higher response speed of the Cu-absorbed ions (Figure 4.6).

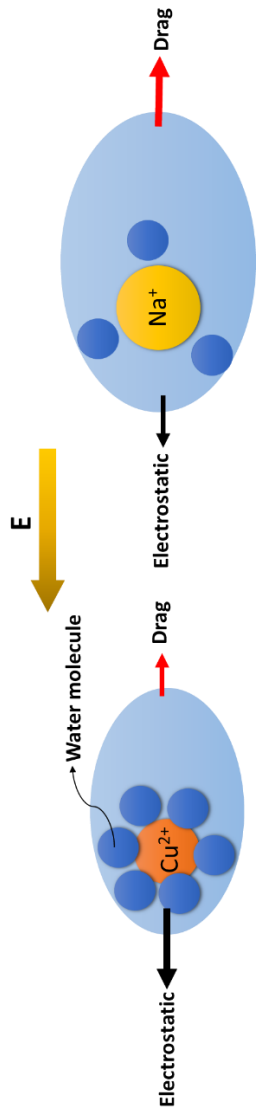

Figure 4.6. Schematics of cupric ion having higher mobility due to lower hydrodynamic radius despite carrying more water molecules

Further, it is reported that despite Cu-ions having a lower hydrodynamic radius, they have a higher solvation number compared to Na-ions. Intuitively higher solvation number means the ions are surrounded by more water molecules [30, 31]. A higher solvation number enables Cu-ions to displace a large number of water molecules which intern increases the osmotic pressure potential generated. The higher osmotic pressure drives more water molecules into the membrane near the positive electrode region increasing the swelling

of this area and subsequently increasing the tip displacement achieved by the ionomer.

4.2. Force characterization

While developing a new actuator it is important to measure the blocking force as it decides the potential application of the actuator. Thus the tip force developed by the actuator by varying the applied electric field and thickness of the actuator was investigated by an in-house experimental setup (Figure 4.7). It is observed that increasing the electric field increases the blocking force of the ionomer in an almost linear trend (Figure 4.8(a)). This is because of the increase in tip displacement of the actuator with the increment in the electric field applied as observed in the previous section. Further, it was observed that the tip force developed by the ionomer is proportional to the square of the thickness which is in line with the results obtained for the IPMC (Figure 4.8(b)). It should be noted that the fitted line has goodness of fit (R^2) above 98% which validates the force characteristic of the actuator. In addition to this, it is noticed that the ion-absorption process increases the tip force developed by the ionomer by atleast two times irrespective of the applied electric field and thickness of the actuator. This may be attributed to the higher charge of copper ions enabling it to replace two sodium ions and thus creating a cross-linking effect and subsequently improving the stiffness of the ionomer. Further, the increased deformation exhibited by Cu-absorbed ionomer could also aid in the observed increase in the generated tip force. From the results, it is inferred that the developed actuator can be successfully applied to soft robotic applications.

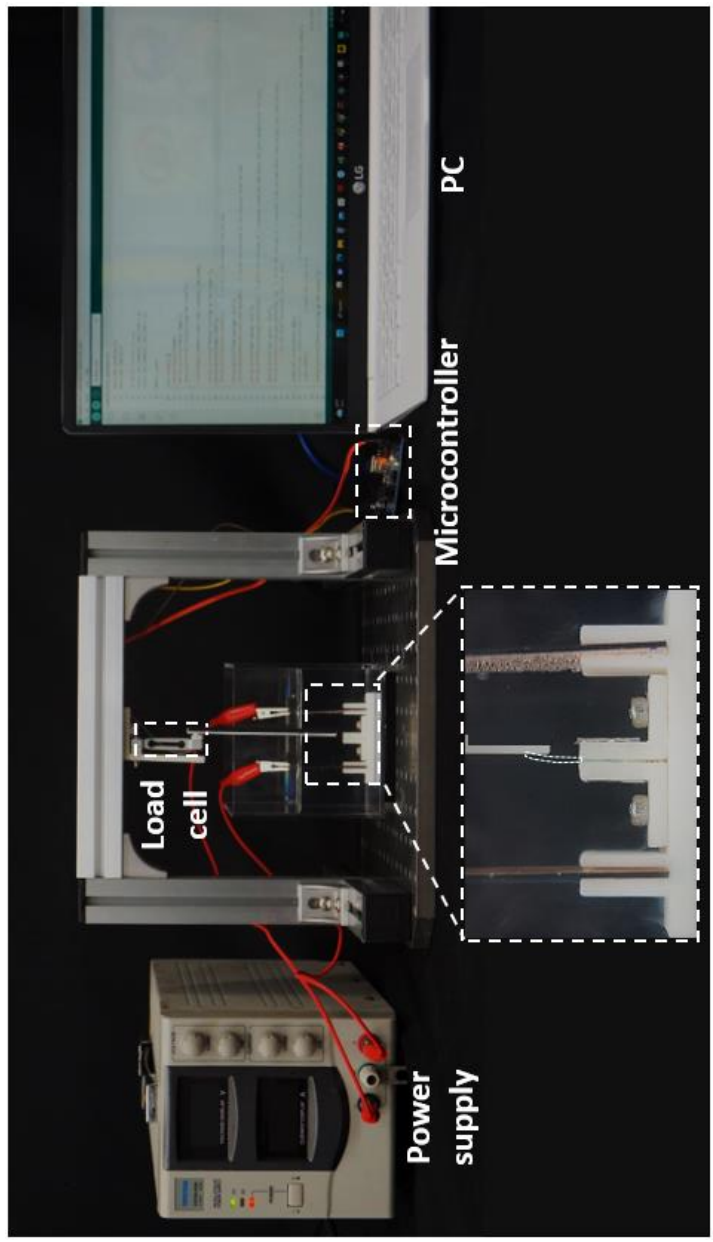

Figure 4.7. Experimental setup for measuring blocking force of ionomer actuator

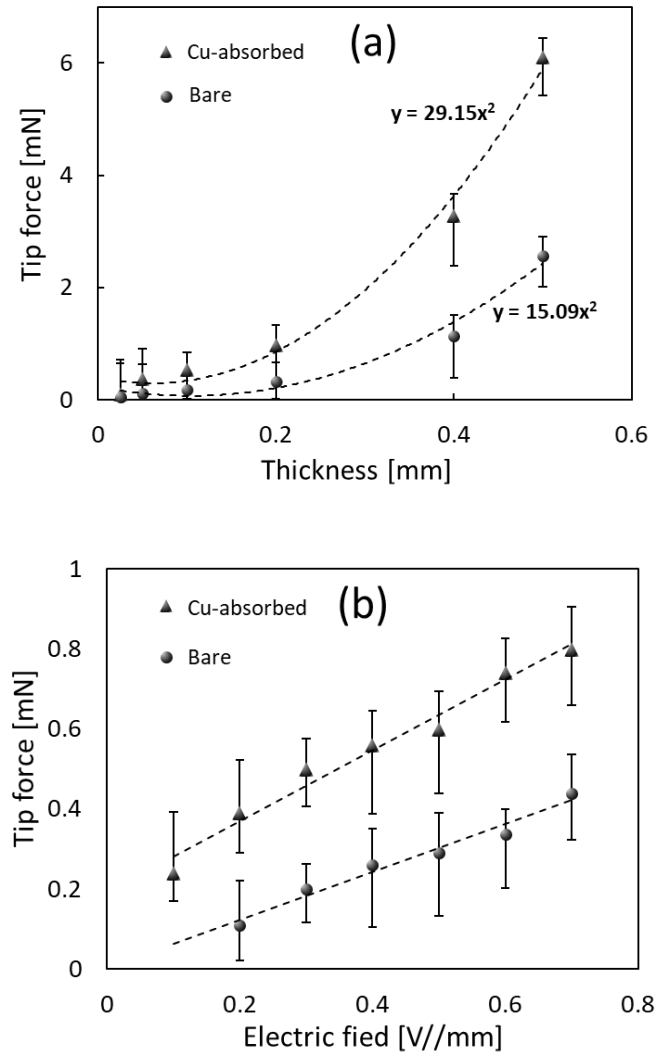

Figure 4.8. Calculation of tip force generated by the ionomer by varying the (a) thickness of the actuator and (b) input electric field

4.3. Response of ionomer to AC signal

Further, given the high response speed of the developed actuator (Cu-absorbed) to the DC signal, the tip displacement of the ionomer for various amplitudes and frequencies of the AC signal is investigated. As expected, the response of the ionomer to the AC signal decreases with an increase in the frequency of the signal with the actuator showing no response above 4 Hz

(figure 4.9). Besides the effect of AC signal amplitude on the deformation of the ionomer is studied. It is noted that the ionomer achieves larger tip displacement at higher rates on increasing the amplitude of the AC signal. This is different from the AC response of the IPMC actuator wherein though the magnitude of displacement increases with input signal amplitude, the time taken to reach the maximum displacement increases. This can be attributed to the difference in response shown by the ionomer actuator and IPMC to DC signal. Although increasing the input voltage (DC) increases the deformation of the IPMC the time to reach this value increases. Whereas, increasing the input electric field (constant) results in an increase in both tip displacement and rate of displacement of the developed actuator.

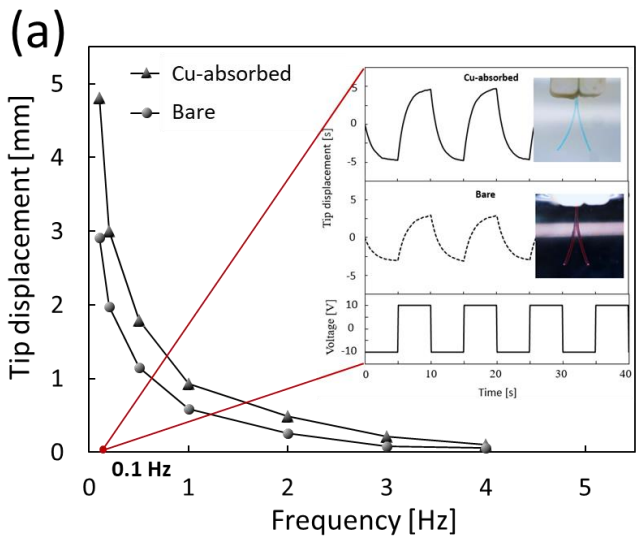

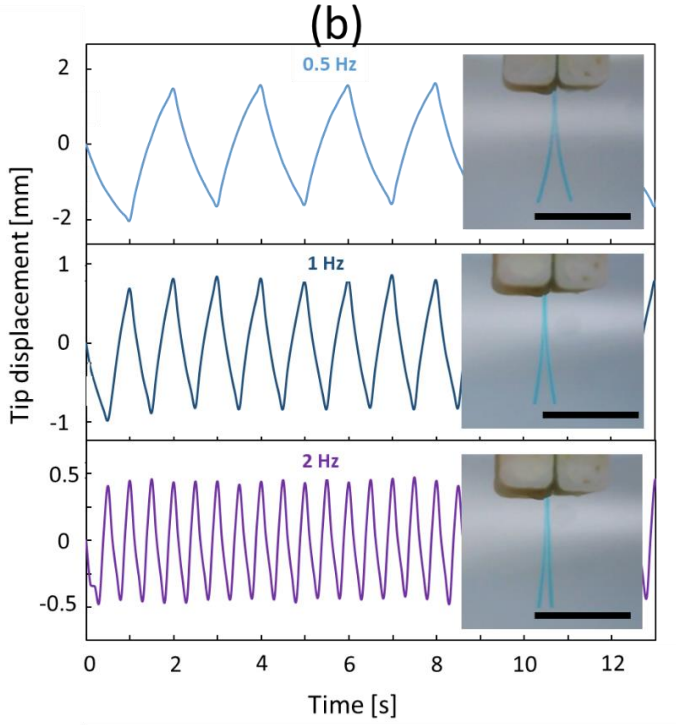
(b)
0.5 Hz
1 Hz
2 Hz
Tip displacement [mm]
Time [s]
2
0
-2
1
0
-1
0.5
0
-0.5
0
2
4
6
8
10
12

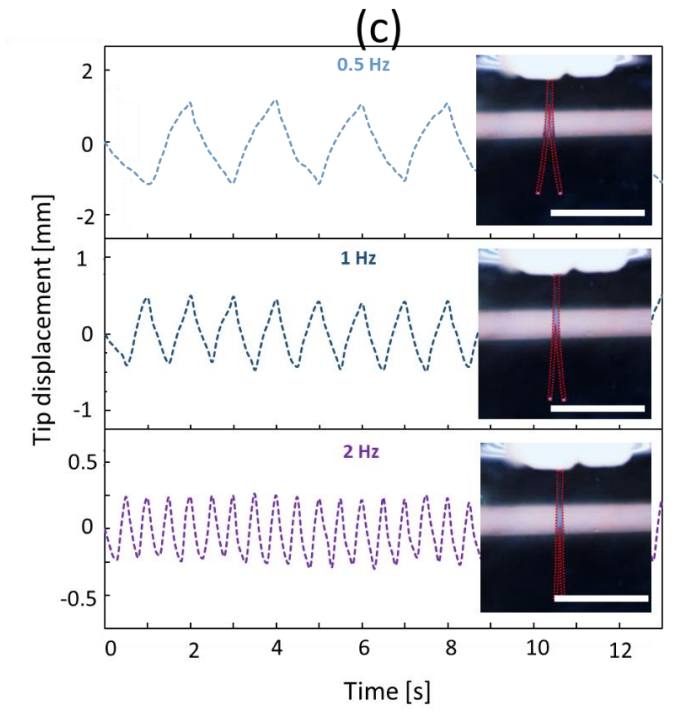
(c)
0.5 Hz
1 Hz
2 Hz
Tip displacement [mm]
Time [s]
2
0
-2
1
0
-1
0.5
0
-0.5
0
2
4
6
8
10
12

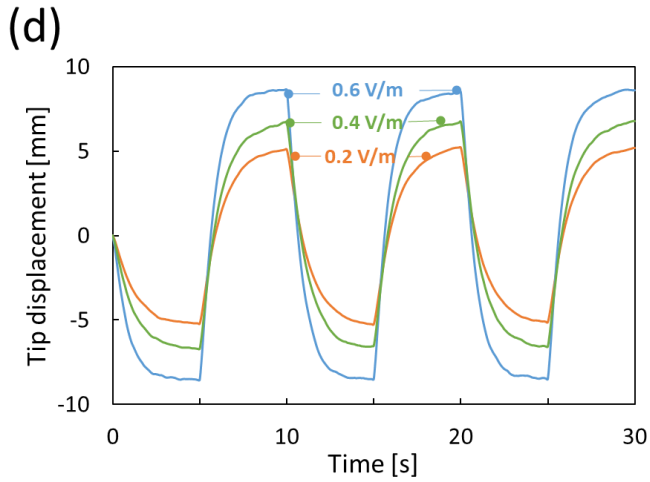

Figure 4.9. Displacement characterization of the ionomer under AC signal with (a) Deformation at different frequency (here insert is the AC response of the ionomer at 0.1 Hz); (b) AC response of the cu-absorbed ionomer actuator; (c) AC response before ion-absorption process (scale bar 5mm); and (d) Deformation at different input electric field at 0.1 Hz.

Chapter 5. Application of ionomer actuator

The potential applications of the ionomer actuator are demonstrated through the development of micro gripper and micro-robotic fish which will be delineated in the following sections

5.1. Two-axis Micro gripper

Based on the force characterization results it was expected that the developed actuator can be used to develop a micro gripper. Hence a two axis micro gripper that could successfully implement pick and place operation is presented. The design of micro gripper consisted of single active arm which was made of the ionic polymer actuator. Whereas the second arm and the entirety of the body are made of ABS and fabricated using extrusion based 3D printing. The dimensions of the micro gripper components are given in Figure 5.1. Further to facilitate the motion of the micro gripper in the x-y plane for pick-and-place operation, it was coupled with automated stages. The gripping action was recorded using a CMOS camera as shown in Figure 5.1. To delineate the mechanism, with the aid of the stage, the micro gripper is initially positioned on top of the particle in the origin location. Further, when forward voltage is applied the active arm moves towards the negative electrode closing the gap between arms, enabling it to grip the object. After the object is griped the micro gripper is moved to the destination using stage and on reaching the destination electric field is removed. The removal of field forces the active arm to go to its initial position releasing the object (figure 5.2(a)). The time-stamps of the micro gripper picking, translating, and placing the object is shown in Figure 5.2 (b) and (c). It must be noted that when the particle size is larger than the distance between the gripper arms extra step is involved during the gripping stage. That is initially a reverse field is applied to open the gap between the two arms to facilitate the gripping of the object on the application of forward field (figure 5.2(c)). Thus, the developed micro gripper could successfully perform the pick and place operation of objects of varying particle sizes ranging from 1 to 3 mm. Thus we envision that the micro gripper be implemented on lab-on-chip systems to manipulate and analyze biological specimens.

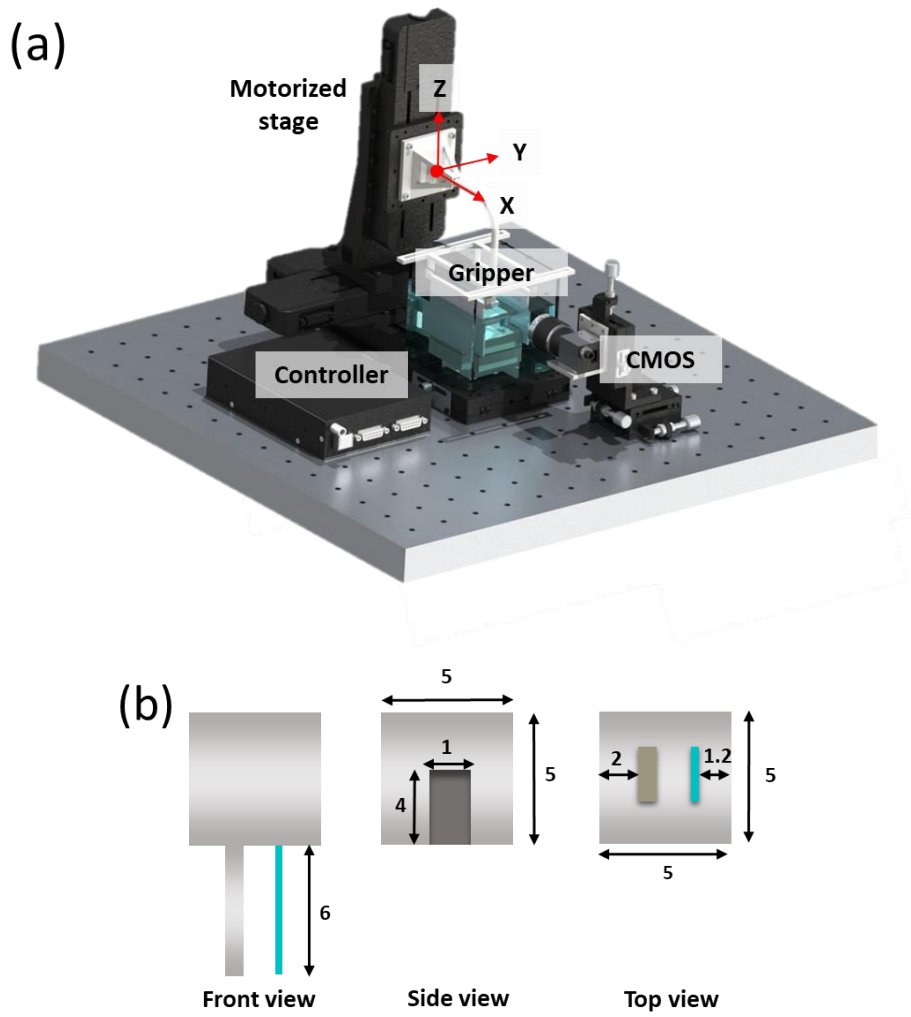

Figure 5.1. Micro gripper configuration for pick and place operation with (a) Experimental setup and (b) Design of the developed micro gripper.

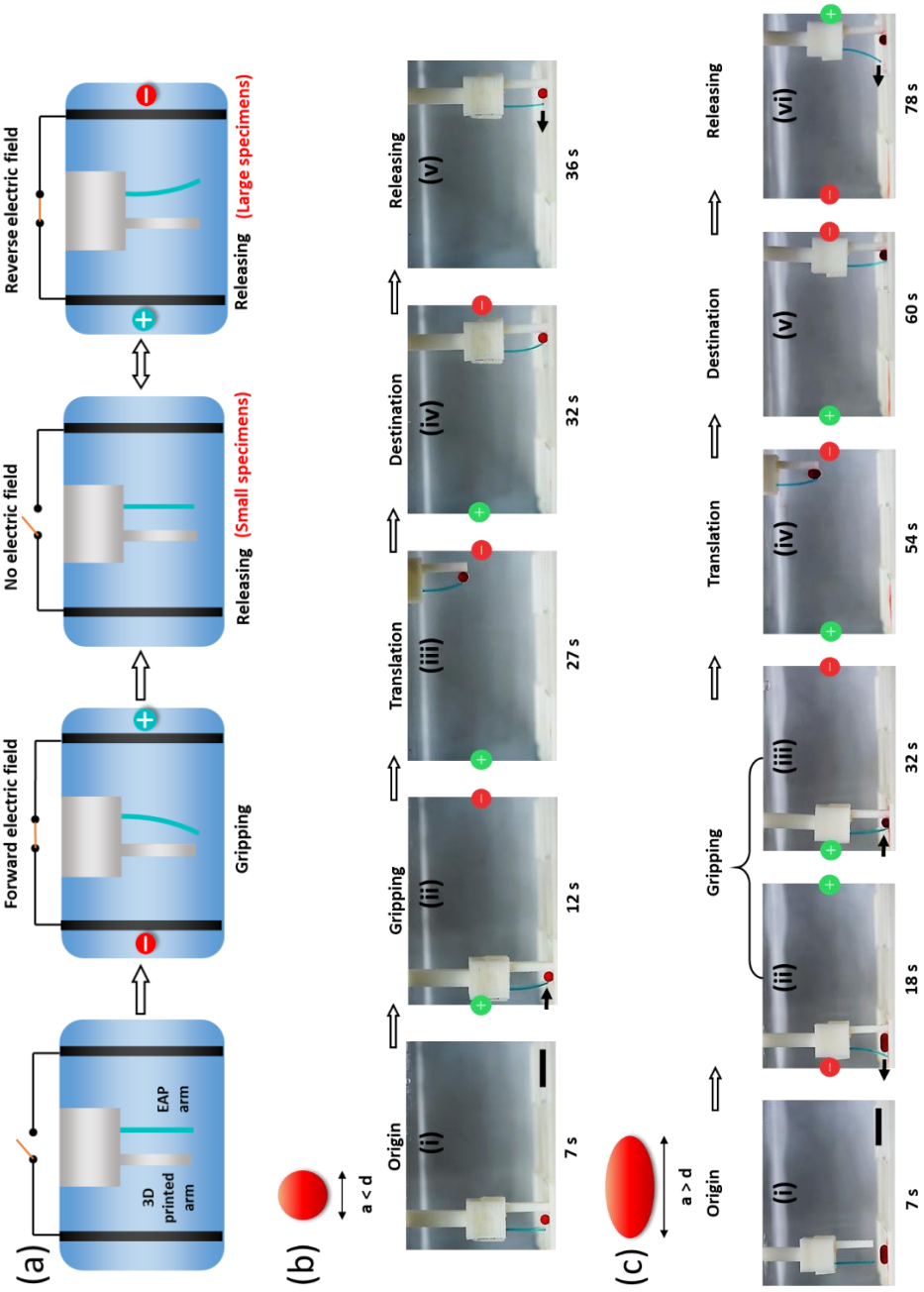

Figure 5.2. Development of gripper using ionomer with (a) Schematics of the gripping mechanism consisting of single active under electric field; (b, c) time stamps of the micro gripper gripping, translating and releasing objects of varying size (here a is the radius of the specimen and d is the distance between the two gripping arms)

5.2. Micro robotic fish

Given the huge potential of untethered aquatic robots for remote drug delivery and surveillance applications over the years researchers have developed numerous electrically driven aquatic robots made of either IPMC or other electroactive polymers. However, the requirement of onboard components resulted in the requirement of large body size which in turn increased the weight and subsequently caused poor performance. Hence, it has been difficult to realize their practical implementation. Therefore, in this study, for the first time, a remote electric field controlled micro robotic fish is considered. As the developed micro robot does not need onboard power and control circuit, the overall length of micro robot is 9 mm and its weight is 40 mg. This is the lightest and smallest aquatic robot that is driven by an electric field ever developed. The design of the micro robotic fish involves, aerodynamically shaped (boat-inspired) fabricated using Stereolithography. Whereas the tail was made of the developed actuator (figure 5.3). Further, an image tracking software was used for all the measurements. To obtain the maximum thrust, the speed of the micro robot with respect to the frequency of the input field is studied. It is noted that for a given field strength, the micro robot reaches maximum speed at 0.5 Hz. Thus, the micro robot was controlled using 0.5 Hz 10 V AC signal using a customized H-bridge circuit. Using remote electric field, the micro robot was made to follow three paths: U, infinite, and circular. The motion of the micro robot was recorded using a DSLR camera as shown in the Figure 5.4(a). The mechanism for controlling the micro robot is represented in Figure 5.4(b). For instance, applying AC field enables the micro robot to move forward due to the generated thrust. Further, as shown in Figure 5.4(b) providing a DC field bends the actuator towards negative potential causing the turning of the micro robot. Further Figure 5.4(f) shows the time lapse images of the micro robot undergoing forward, turning and backward motion to traverse U path. During the U-path, it is noted that the developed micro robot can reach a maximum speed of 0.42 Bl/s (with tail) during straight motion and a maximum angular speed of 22.63 deg/s (Figure 5.5 (b) and 5.5 (c)). Moreover, the following of a more complicated infinity path was accomplished by combining turning and straight ward motion. As seen in the Figure 5.6, the maximum velocity of the

micro robotic fish remained almost the same with maximum speeds up to 0.38 Bl/s. Thus it can be observed that robot can be controlled by remote electric field to almost traverse complicated paths. Finally, the developed micro robot is controlled to traverse a circular path (Figure 5.7). During the circular motion the micro robot almost traversed 360 deg with a maximum angular velocity of 24.2 deg/s (Figure 5.7(a) and (b)). It must be noted here that though currently the path travelled is not close to the desired path it is expected by improving the control of delivering input current to remote electrodes the micro robot can be made to traverse paths accurately. Due to the lightweight and simple design, it is envisioned that the developed micro robotic fish can be implemented to deliver drugs in-vivo or in-vitro systems.

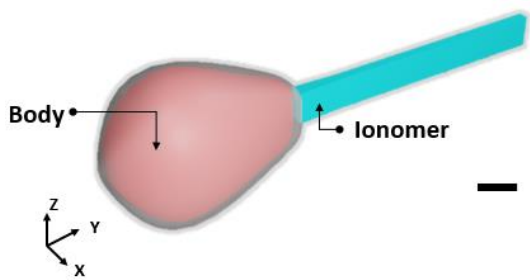

Figure 5.3. Schematics of the design of the micro robotic fish (scale bar is 1 mm)

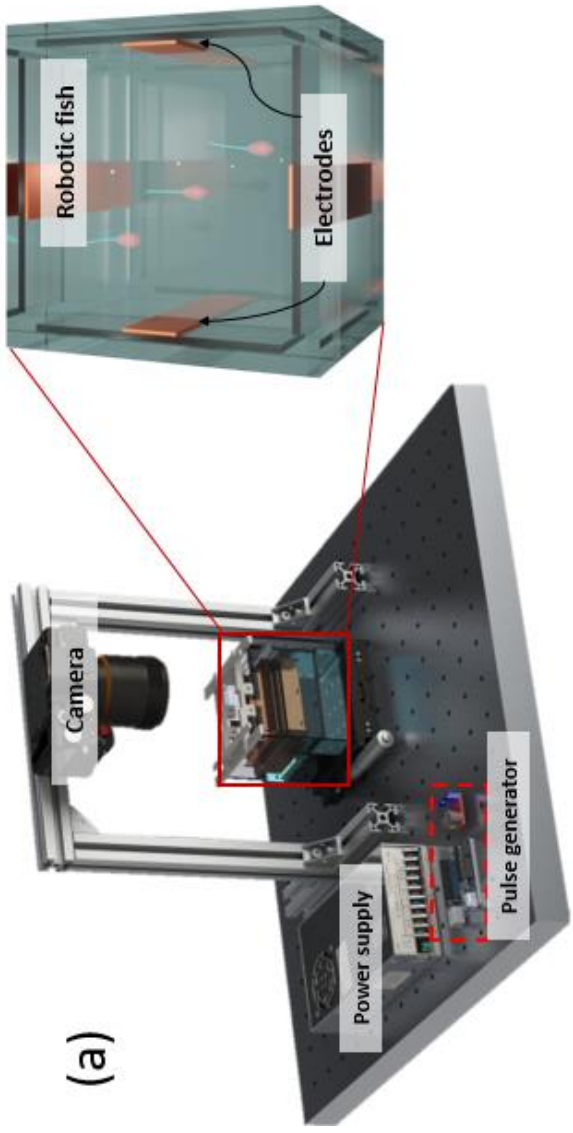
Robotic fish
Electrodes
Camera
Power supply
Pulse generator
(a)

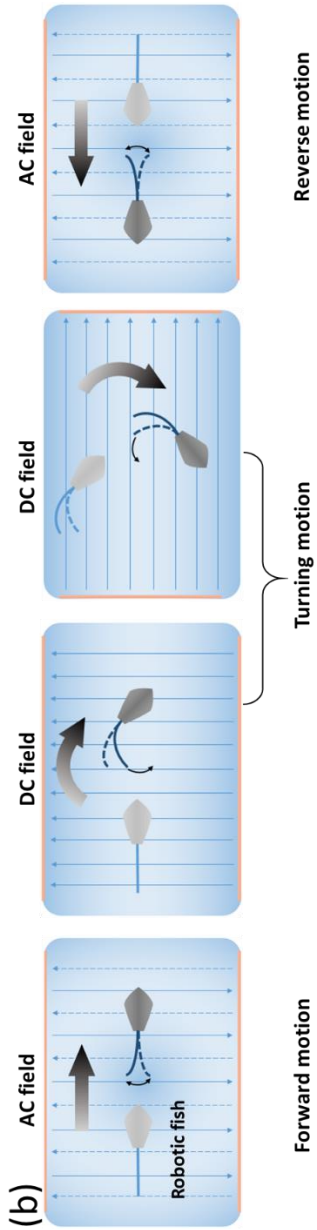

Figure 5.4. Field controlled micro robotic fish with (a) Schematics of the experimental setup (insert presents the tank in which micro robot's motion was observed); (b) Moving mechanism of the micro robot using AC field for straight ward motion and DC field for turning motion.

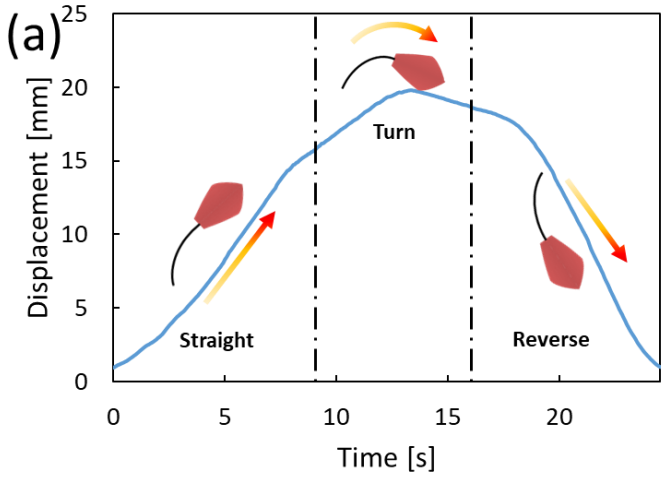
(a)
Displacement [mm]
25
20
15
10
5
0
0
5
10
15
20
Time [s]
Straight
Turn
Reverse

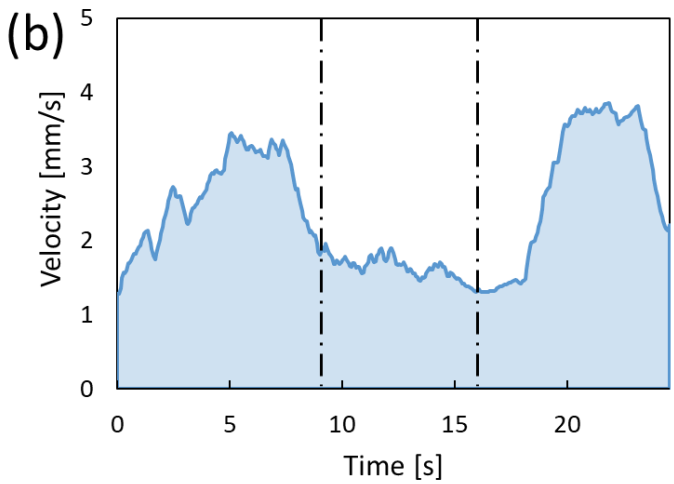
(b)
Velocity [mm/s]
5
4
3
2
1
0
0
5
10
15
20
Time [s]

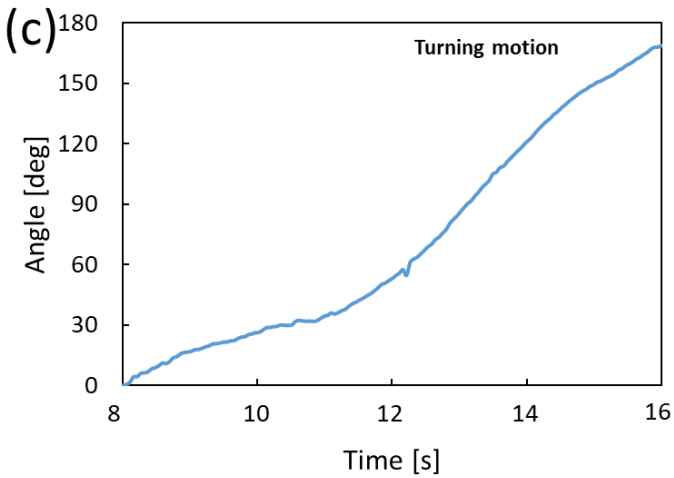
(c)
Angle [deg]
180
150
120
90
60
30
0
8
10
12
14
16
Time [s]
Turning motion

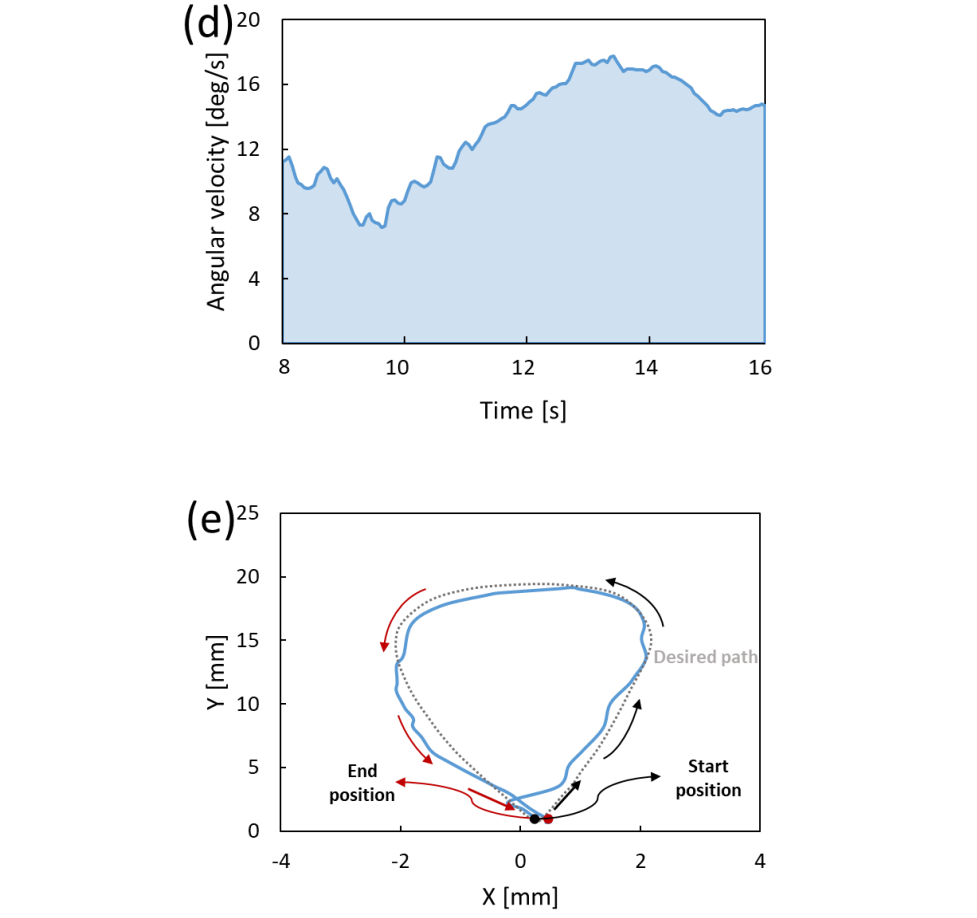

Figure 5.5. Micro robotic fish traversing U path. (a) Displacement travelled by the micro robot; (b) Instantaneous velocity of the micro robot throughout the entire path; (c) Steering angle during the turning motion; (d) Angular velocity during the turning motion; (d) Comparison of the swimming trajectory traversed by the micro robot with desired path; and (f) Time lapse of micro robot following U trajectory (scale bar is 5 mm).

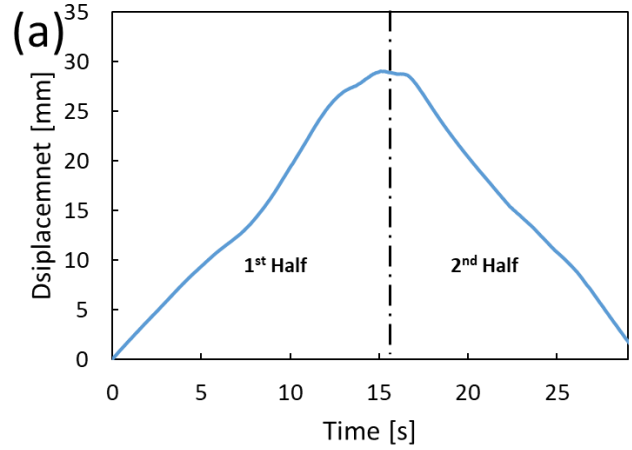
(a)
Dsiplacemnet [mm]
35
30
25
20
15
10
5
0
1st Half
2nd Half
0
5
10
15
20
25
Time [s]

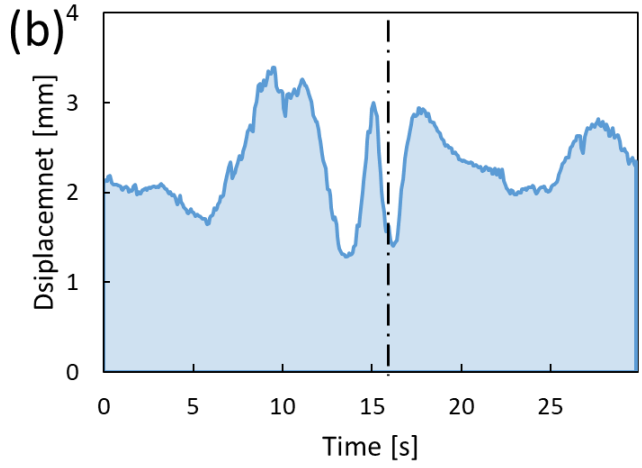
(b)
Dsiplacemnet [mm]
4
3
2
1
0
0
5
10
15
20
25
Time [s]

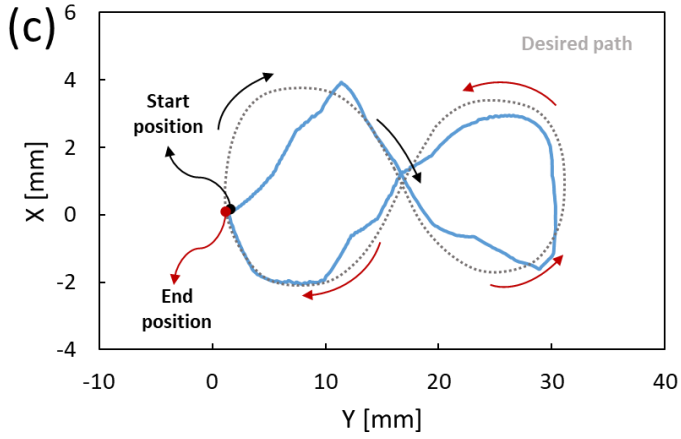
(c)
Desired path
Start position
End position
X [mm]
6
4
2
0
-2
-4
-10
0
10
20
30
40
Y [mm]

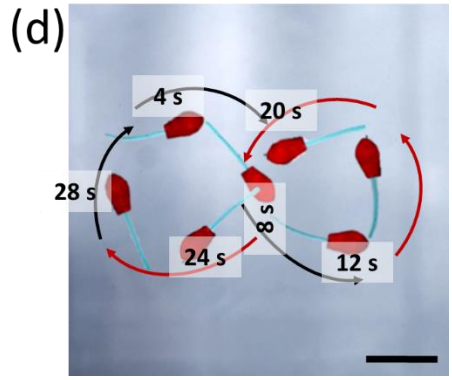

Figure 5.6. Micro robotic fish traversing infinite path. (a) Displacement travelled by the micro robot; (b) Instantaneous velocity of the micro robot throughout the entire path; (c) Comparison of the swimming trajectory traversed by the micro robot with desired path; and (d) Time lapse of micro robot following infinity trajectory (scale bar is 5 mm)

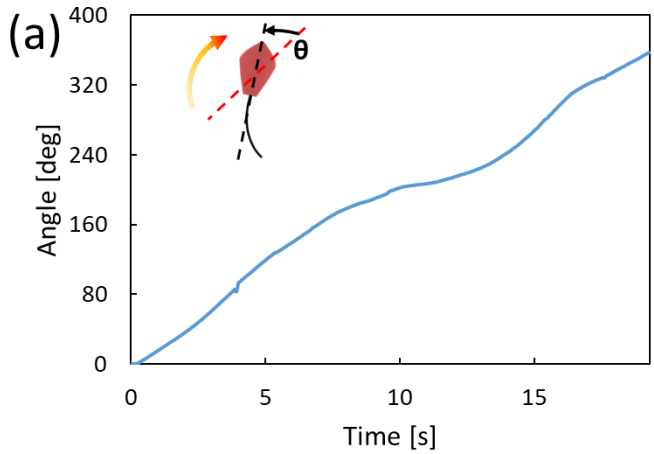

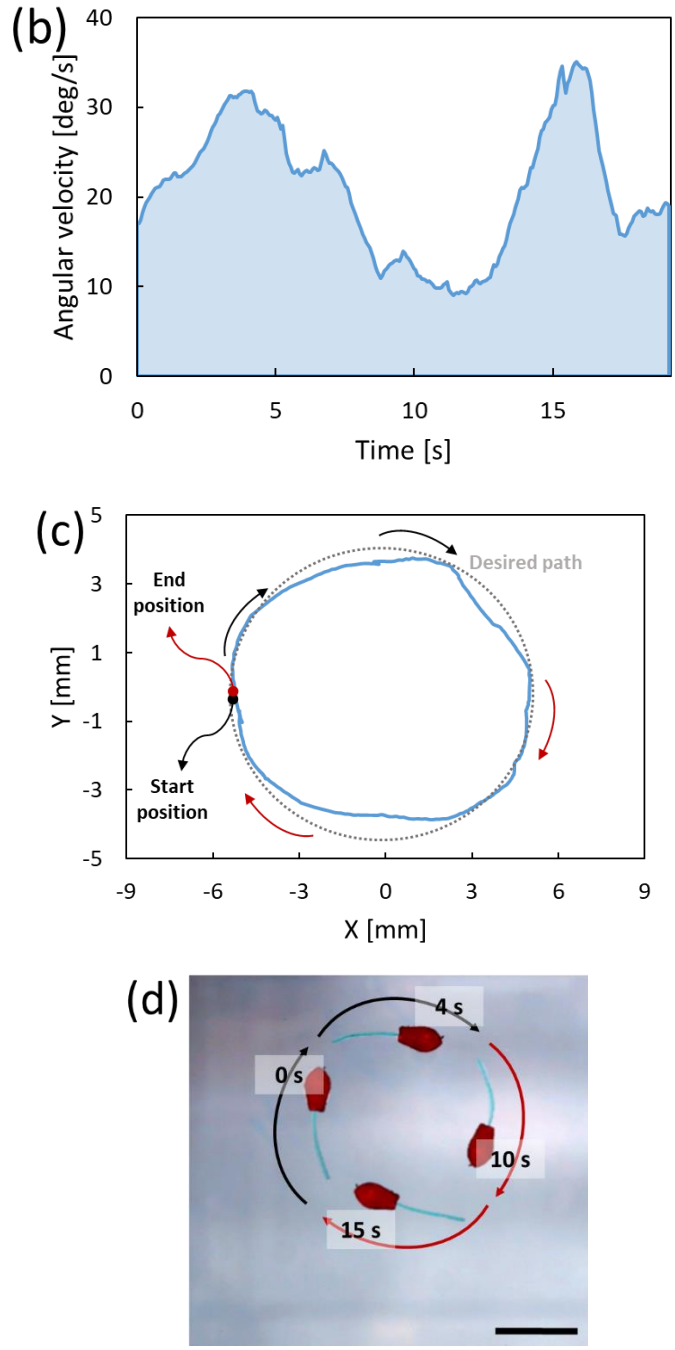

Figure 5.7. Micro robotic fish traversing circular path. (a) Angle travelled by the micro robot; (b) Angular velocity of the micro robot throughout the entire path; (c) Comparison of the swimming trajectory traversed by the micro robot with desired path; and (d) Time lapse of micro robot following infinity trajectory (scale bar is 5 mm)

Chapter 6. Conclusion

In this study, the deformation of an EAP-based actuator in electrolyte solution using low remote electric field. The actuator was fabricated and evaluated for various structural and operation parameters. The deformation of the actuator towards the negative electrode was due to the combined effect of electrophoresis and osmotic pressure. It is noticed that the deformation of the ionomer actuator varies linearly with applied voltage. Whereas the tip displacement of the actuator had non-linear relation with actuator thickness, decreasing beyond a certain value. Further, the study also demonstrates the incorporation of high charge density ions into the ionomer and compares the performance with the unabsorbed actuator. The ion-absorption process increased the actuation speed of the ionomer by atleast three times and the tip force developed by two times irrespective of the applied voltage.

To demonstrate the application of the developed actuator in the field of soft robotics, a micro gripper and a micro robotic fish were designed and fabricated. The micro gripper could successfully pick and place particles of dimensions varying from 1 to 3 mm in diameter using electric field of 0.1 V/m.

Whereas the micro robot could transverse complicated trajectories such as U, circular and infinity. Further, the developed robot was capable of achieving speeds up to 0.42 Bl/s (w tail) and 0.96 Bl/s (w/o tail) (Figure 6.1).

Due to the simple and lightweight design, and untethered nature of power delivery, we envision that the developed micro robot and micro gripper can be implemented in the biomedical field for therapeutic drug delivery or manipulation of biological samples in lab-on-chip systems.

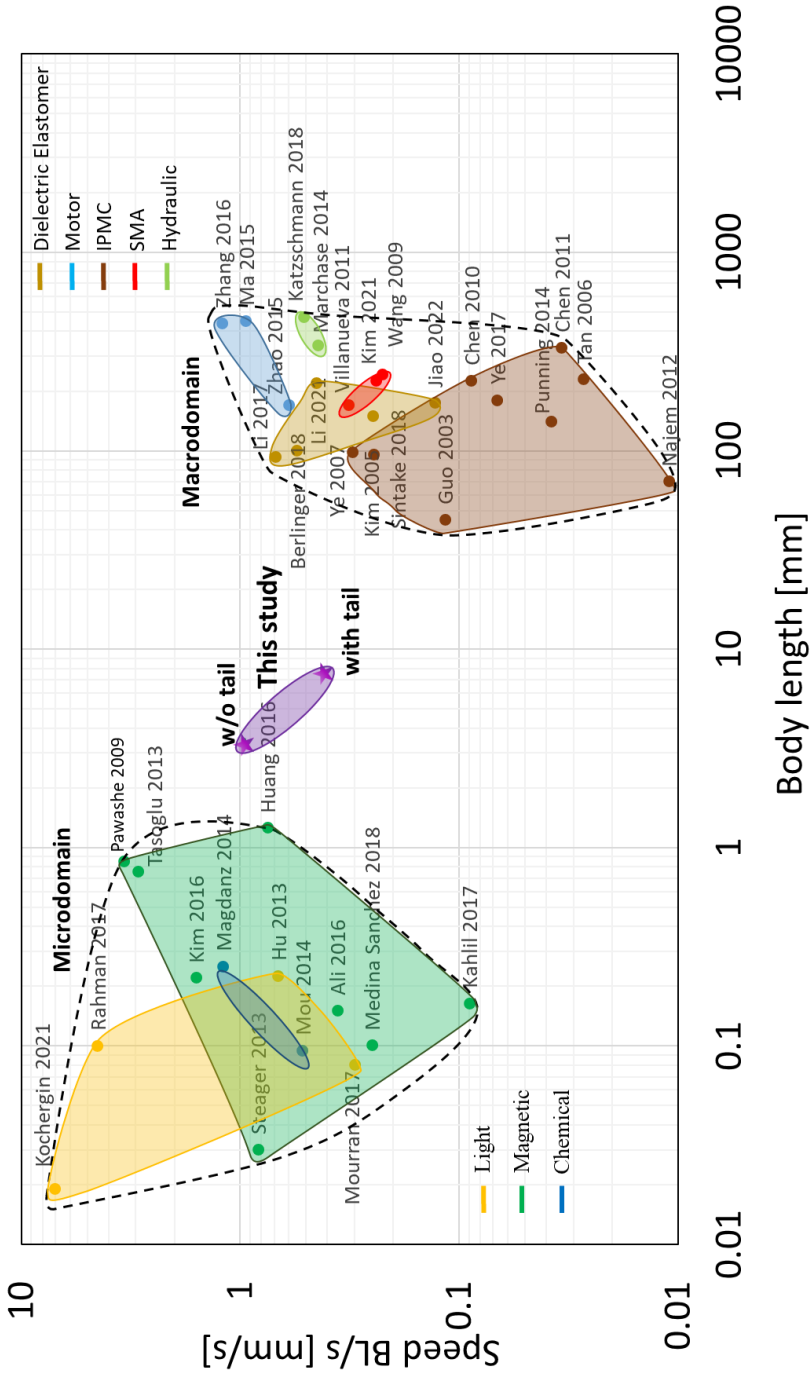

Figure 6.1. Velocity of various aquatic robots in body length per second versus body length [14, 15, 32-63].

Bibliography

1. Yin, Y. and J.A. Rogers, *Introduction: Smart Materials.* Chemical Reviews, 2022. **122**(5): p. 4885-4886.
2. Liu, C., et al., *3D printable and fringe electric field adhesion enabled variable stiffness artificial muscles for semi-active vibration attenuation.* Soft Matter, 2021. **17**(28): p. 6697-6706.
3. Cooper, C.B., et al., *High Energy Density Shape Memory Polymers Using Strain-Induced Supramolecular Nanostructures.* ACS Central Science, 2021. **7**(10): p. 1657-1667.
4. Hunter, I.W. and S. Lafontaine. *A comparison of muscle with artificial actuators*. in *Technical Digest IEEE Solid-State Sensor and Actuator Workshop*. 1992.
5. Bar-Cohen, Y., *Electroactive Polymers as Artificial Muscles - Reality and Challenges.* 19th AIAA Applied Aerodynamics Conference, 2001.
6. Bar-Cohen, Y. and Q. Zhang, *Electroactive Polymer Actuators and Sensors.* MRS Bulletin, 2008. **33**(3): p. 173-181.
7. Shahinpoor, M., et al., *Ionic polymer-metal composites (IPMCs) as biomimetic sensors, actuators and artificial muscles - a review.* Smart Materials and Structures, 1998. **7**(6): p. R15.
8. Bhandari, B., G.-Y. Lee, and S.-H. Ahn, *A review on IPMC material as actuators and sensors: Fabrications, characteristics and applications.* International Journal of Precision Engineering and Manufacturing, 2012. **13**(1): p. 141-163.
9. He, Q., et al., *Review on Improvement, Modeling, and Application of Ionic Polymer Metal Composite Artificial Muscle.* Journal of Bionic Engineering, 2022. **19**(2): p. 279-298.
10. Ma, S., et al., *High-performance ionic-polymer–metal composite: toward large-deformation fast-response artificial muscles.* Advanced Functional Materials, 2020. **30**(7): p. 1908508.
11. Yamakita, M., et al. *A snake-like swimming robot using IPMC actuator and verification of doping effect*. in *2005 IEEE/RSJ International Conference on Intelligent Robots and Systems*. 2005.
12. Bar-Cohen, Y., *Biologically Inspired Intelligent Robots Using*

Artificial Muscles. Vol. 30. 2003. 2.

13. Chen, Z., *A review on robotic fish enabled by ionic polymer–metal composite artificial muscles.* Robotics and biomimetics, 2017. **4**(1): p. 24.
14. Najem, J., et al., *Biomimetic jellyfish-inspired underwater vehicle actuated by ionic polymer metal composite actuators.* Smart Materials and Structures, 2012. **21**(9): p. 094026.
15. Ye, Z., et al., *2D maneuverable robotic fish propelled by multiple ionic polymer–metal composite artificial fins.* International Journal of Intelligent Robotics and Applications, 2017. **1**(2): p. 195-208.
16. Fleming, M.J., K.J. Kim, and K.K. Leang, *Mitigating IPMC back relaxation through feedforward and feedback control of patterned electrodes.* Smart Materials and Structures, 2012. **21**(8): p. 085002.
17. Annabestani, M., et al. *Eliminating Back Relaxation in Large-Deformable IPMC Artificial Muscles: A Noise-Assistive Pattern-Free Electrode Approach*. in *2020 27th National and 5th International Iranian Conference on Biomedical Engineering (ICBME)*. 2020.
18. Guo, D., et al., *PEDOT coating enhanced electromechanical performances and prolonged stable working time of IPMC actuator.* Sensors and Actuators B: Chemical, 2020. **305**: p. 127488.
19. Yu, C.-Y., Y.-W. Zhang, and G.-D.J. Su, *Reliability tests of ionic polymer metallic composites in dry air for actuator applications.* Sensors and Actuators A: Physical, 2015. **232**: p. 183-189.
20. Lee, S.-G., et al., *Performance Improvement of IPMC (Ionic Polymer Metal Composites) for a Flapping Actuator.* International Journal of Control, Automation and Systems, 2006. **4**.
21. Lee, J.-W., S.M. Hong, and C.M. Koo, *High-performance polymer ionomer–ionic liquid membrane IPMC actuator.* Research on Chemical Intermediates, 2014. **40**(1): p. 41-48.
22. Chang, X.L., et al., *Radio-frequency enabled ionic polymer metal composite (IPMC) actuator for drug release application.* Smart Materials and Structures, 2019. **28**(1): p. 015024.
23. Kim, M.J., et al., *Effects of ionic liquids on the performance of IPMC*. SPIE Smart Structures and Materials + Nondestructive Evaluation and Health Monitoring. Vol. 10163. 2017: SPIE.

24. Han, D., et al., *Soft Robotic Manipulation and Locomotion with a 3D Printed Electroactive Hydrogel.* ACS Applied Materials & Interfaces, 2018. **10**(21): p. 17512-17518.
25. Mohsen, S. and J.K. Kwang, *Ionic polymer–metal composites: III. Modeling and simulation as biomimetic sensors, actuators, transducers, and artificial muscles.* Smart Materials and Structures, 2004. **13**(6): p. 1362.
26. Newbury, K.M. and D.J. Leo, *Linear electromechanical model of ionic polymer transducers - Part I: Model development.* Journal of Intelligent Material Systems and Structures, 2003. **14**: p. 333-342.
27. Gennes, P.G.d., et al., *Mechanoelectric effects in ionic gels.* Europhysics Letters, 2000. **50**(4): p. 513.
28. Flory, P.J., *Principles of polymer chemistry*. 1953: Cornell university press.
29. Kadhim, M.J. and M.I. Gamaj. *Estimation of the Diffusion Coefficient and Hydrodynamic Radius (Stokes Radius) for Inorganic Ions in Solution Depending on Molar Conductivity as Electro-Analytical Technique-A Review*. 2020.
30. Peng, J., et al., *The effect of hydration number on the interfacial transport of sodium ions.* Nature, 2018. **557**(7707): p. 701-705.
31. Bowron, D.T., et al., *The hydration structure of Cu2+: more tetrahedral than octahedral?* RSC Advances, 2013. **3**(39): p. 17803-17812.
32. Chen, Z., S. Shatara, and X. Tan, *Modeling of Biomimetic Robotic Fish Propelled by An Ionic Polymer–Metal Composite Caudal Fin.* IEEE/ASME Transactions on Mechatronics, 2010. **15**(3): p. 448-459.
33. Chen, Z., et al. *Bio-Inspired Robotic Cownose Ray Propelled by Electroactive Polymer Pectoral Fin*. in *ASME 2011 International Mechanical Engineering Congress and Exposition*. 2011.
34. Shuxiang, G., T. Fukuda, and K. Asaka, *A new type of fish-like underwater microrobot.* IEEE/ASME Transactions on Mechatronics, 2003. **8**(1): p. 136-141.
35. Kim, B., et al., *A biomimetic undulatory tadpole robot using ionic polymer–metal composite actuators.* Smart Materials and Structures, 2005. **14**(6): p. 1579.

36. Tan, X., et al. *An Autonomous Robotic Fish for Mobile Sensing*. in *2006 IEEE/RSJ International Conference on Intelligent Robots and Systems*. 2006.
37. Villanueva, A., C. Smith, and S. Priya, *A biomimetic robotic jellyfish (Robojelly) actuated by shape memory alloy composite actuators.* Bioinspiration & Biomimetics, 2011. **6**(3): p. 036004.
38. Wang, Z., et al. *A micro biomimetic manta ray robot fish actuated by SMA*. in *2009 IEEE International Conference on Robotics and Biomimetics (ROBIO)*. 2009.
39. Xiufen, Y., S. Yudong, and G. Shuxiang. *A centimeter-scale autonomous robotic fish actuated by IPMC actuator*. in *2007 IEEE International Conference on Robotics and Biomimetics (ROBIO)*. 2007.
40. Zhao, Y., et al., *Performance of Very Small Robotic Fish Equipped with CMOS Camera.* Robotics, 2015. **4**(4): p. 421-434.
41. Kim, H.-S., et al., *Shape memory alloy-driven undulatory locomotion of a soft biomimetic ray robot.* Bioinspiration & Biomimetics, 2021. **16**(6): p. 066006.
42. Cai, Y., et al., *A biomimetic cownose ray robot fish with oscillating and chordwise twisting flexible pectoral fins.* Industrial Robot: An International Journal, 2015. **42**.
43. Katzschmann, R.K., et al., *Exploration of underwater life with an acoustically controlled soft robotic fish.* Science Robotics, 2018. **3**(16): p. eaar3449.
44. *Autonomous Soft Robotic Fish Capable of Escape Maneuvers Using Fluidic Elastomer Actuators.* Soft Robotics, 2014. **1**(1): p. 75-87.
45. Zhang, S., et al., *Design and Control of an Agile Robotic Fish With Integrative Biomimetic Mechanisms.* IEEE/ASME Transactions on Mechatronics, 2016. **21**(4): p. 1846-1857.
46. *Soft Biomimetic Fish Robot Made of Dielectric Elastomer Actuators.* Soft Robotics, 2018. **5**(4): p. 466-474.
47. Jiao, Z.-W., et al., *A BCF Bionic Robot Fish Driven by A Dielectric Elastomer Actuator.* Journal of Physics: Conference Series, 2022. **2331**(1): p. 012010.
48. Li, T., et al., *Fast-moving soft electronic fish.* Science Advances, 2017.

3(4): p. e1602045.

49. Berlinger, F., et al. *A Modular Dielectric Elastomer Actuator to Drive Miniature Autonomous Underwater Vehicles*. in *2018 IEEE International Conference on Robotics and Automation (ICRA)*. 2018.
50. Li, G., et al., *Self-powered soft robot in the Mariana Trench.* Nature, 2021. **591**(7848): p. 66-71.
51. Huang, H.-W., et al., *Soft micromachines with programmable motility and morphology.* Nature Communications, 2016. **7**(1): p. 12263.
52. Magdanz, V., et al., *Stimuli-Responsive Microjets with Reconfigurable Shape.* Angewandte Chemie International Edition, 2014. **53**(10): p. 2673-2677.
53. Mou, F., et al., *Autonomous Motion and Temperature-Controlled Drug Delivery of Mg/Pt-Poly(N-isopropylacrylamide) Janus Micromotors Driven by Simulated Body Fluid and Blood Plasma.* ACS Applied Materials & Interfaces, 2014. **6**(12): p. 9897-9903.
54. Garcia-Gradilla, V., et al., *Ultrasound-Propelled Nanoporous Gold Wire for Efficient Drug Loading and Release.* Small, 2014. **10**(20): p. 4154-4159.
55. Magdanz, V., et al., *Dynamic Polymeric Microtubes for the Remote-Controlled Capture, Guidance, and Release of Sperm Cells.* Advanced Materials, 2016. **28**(21): p. 4084-4089.
56. Khalil, I.S.M., et al. *Swimming in low reynolds numbers using planar and helical flagellar waves*. in *2017 IEEE/RSJ International Conference on Intelligent Robots and Systems (IROS)*. 2017.
57. Medina-Sánchez, M., et al., *Swimming Microrobots: Soft, Reconfigurable, and Smart.* Advanced Functional Materials, 2018. **28**(25): p. 1707228.
58. Mourran, A., et al., *Soft Microrobots Employing Nonequilibrium Actuation via Plasmonic Heating.* Advanced Materials, 2017. **29**(2): p. 1604825.
59. Chen, X.Z., et al., *Hybrid magnetoelectric nanowires for nanorobotic applications: fabrication, magnetoelectric coupling, and magnetically assisted in vitro targeted drug delivery.* Advanced Materials, 2017. **29**(8): p. 1605458.
60. Rahman, M.A., et al., *Cooperative Micromanipulation Using the*

Independent Actuation of Fifty Microrobots in Parallel. Scientific Reports, 2017. **7**(1): p. 3278.

61. Chen, Y., et al., *Controllable water surface to underwater transition through electrowetting in a hybrid terrestrial-aquatic microrobot.* Nature Communications, 2018. **9**(1): p. 2495.
62. Hu, W., et al. *Bubble-driven light-absorbing hydrogel microrobot for the assembly of bio-objects*. in *2013 35th Annual International Conference of the IEEE Engineering in Medicine and Biology Society (EMBC)*. 2013.
63. Kim, S., et al., *Fabrication and manipulation of ciliary microrobots with non-reciprocal magnetic actuation.* Scientific reports, 2016. **6**(1): p. 1-9.